The thermodynamic uncertainty relation in the three-level laser with a quantized field

Master's Thesis

Autor: Sander Stammbach

Supervisors: Prof. Patrick Potts, Dr. Mateo Brunelli, Marcelo Janovitch,

Date: 30.3.2024

Abstract

This thesis investigates the behavior of heat and cavity heat current, as well as power generation, in a three-level quantum system in a cavity, coupled to a thermal bath and external field. Three different methods are employed, including the derivation and solution of Heisenberg equations of motion, yielding results consistent with numerical simulations. The analysis focuses on the heat current's dependency on external field strength, coupling constant, and temperature, with comparisons made to previous works. Notably, a double-threshold behavior in heat current is observed with varying parameters. Additionally, the influence of external conditions, such as temperature and coherent field detuning, on heat current and power generation is explored, revealing the double-threshold behavior under specific conditions. By investigating the thermodynamic uncertainty relation (TUR) we found minimal entropy production rates and variances for the heat current. We examined all parameters concerning the violation of the thermodynamic uncertainty relation and found explanations by considering the entropy production for why the TUR is not violated in this system. Comparison with existing models demonstrates the influence of external factors on thermodynamic behaviors, with the cavity's impact on cavity heat current and entropy production highlighted.

1 Acknowledgements

Completing my master's thesis was made possible through the consistent support and guidance generously provided by my supervisor, Prof. Patrick Potts. His direct yet compassionate approach not only navigated me through the diverse challenges of my master's thesis but also made the journey thoroughly gratifying, culminating in its successful completion. I express immense gratitude for his invaluable support. Special thanks are also due to Matteo Brunelli and Marcelo Janovitch, who not only supervised my master's project but also provided invaluable assistance and guidance with technical intricacies throughout the entire process. Furthermore, I extend my gratitude to Marcelo Janovitch for helping me many times to improve my writing, offering insightful references relevant to the topics covered in my thesis, and warmly welcoming further exploration and exchange of ideas. Their contributions were immensely appreciated and significantly enriched the depth of my research. I would like to express my sincere appreciation to all mentioned for their unwavering support, guidance, and scholarly camaraderie throughout this academic journey.

Contents

1 Acknowledgements **1**

2 Introduction **3**

3 System and Model **4**
3.1 Rotating frame 6

4 Equations of motion **6**
4.1 Factorization 6
4.2 Approximation for high external field strength f 7
4.3 Heat current versus external field 7

5 Laws of thermodynamic **8**
5.1 First law of thermodynamic 8
5.1.1 Equations of motion 9
5.2 Second law 10

6 Double-threshold behavior and population inversion **11**
6.1 Wigner functions 13

7 Influence of the external field **14**
7.1 cavity heat current and Power 14
7.2 Non-linear behavior 15
7.3 Wigner function 17

8 Thermodynamic Uncertainty Relation **18**
8.1 Full counting statistics 18
8.2 TUR investigations 20

9 Conclusion **23**

A Rotating frame transformation **25**

B Equations of motion **26**

C Full counting statistics **27**
C.1 Vectorisation 27

2 Introduction

Heat engines have been of interest since the industrialization period. The concept involves converting thermal energy into an electromagnetic wave, which can then be utilized. These can also be implemented in quantum systems. The three-level maser is an example of a concept but is already non-classical. Converting thermal energy with a three-level quantum system was adopted by Schulz-Dubois [1], where the energy output is a state of light wave. In other words, it is possible to build a laser that is driven by the interaction with a hot and cold reservoir. This thesis analyzes a modified form of such a three-level laser. Compared to the previous version [2], the modification is that this three-level system is placed in a cavity and can be driven by an external field. To gain as much knowledge as possible about this quantum heat engine, various aspects are discussed in this thesis. The calculations were performed both analytically using the approximated equations of motion and numerically. First, we analyze the heat current J_h and J_c, the cavity heat current J_{cav}, and the power P, of their behavior when parameters change.

Second, we consider the fluctuations of heat, in order to investigate the validity of the *thermodynamic uncertainty relation*, emphasis is placed on the differences between [2] and this thesis. Unlike [2], our system is situated within a cavity. We examine the thermodynamic uncertainty in detail in the three-level laser about all the relevant parameters of the master equation. TUR violation would allow us to identify operating regimes where quantum dynamics lead to improved performance quantified by a lower value of the TUR as the classical limit.

For the average heat current, we found a double-threshold behavior which is described in [3] and can only be described quantum mechanically. The question that arises and that we investigate is how the external field affects the system and changes the cavity heat current and power. We also investigate the non-linear behavior of the expected value of the ladder operator $\langle a \rangle$ and compare it to the analytical solution outlined in [4]. We investigate all the parameters that describe our three-level laser and find an optimum. Similar to the work by [2], our three-level system is also coupled to a hot and cold bath. Additionally, it is also driven by an external field. In comparison to [2] approach, the three-level system is situated within a cavity. This leads to a state of light from a PHAV state to a coherent state 10, as well as a change in the circumstances under which the TUR is minimal. We found out, that we have no TUR violation in the presence of the cavity.

3 System and Model

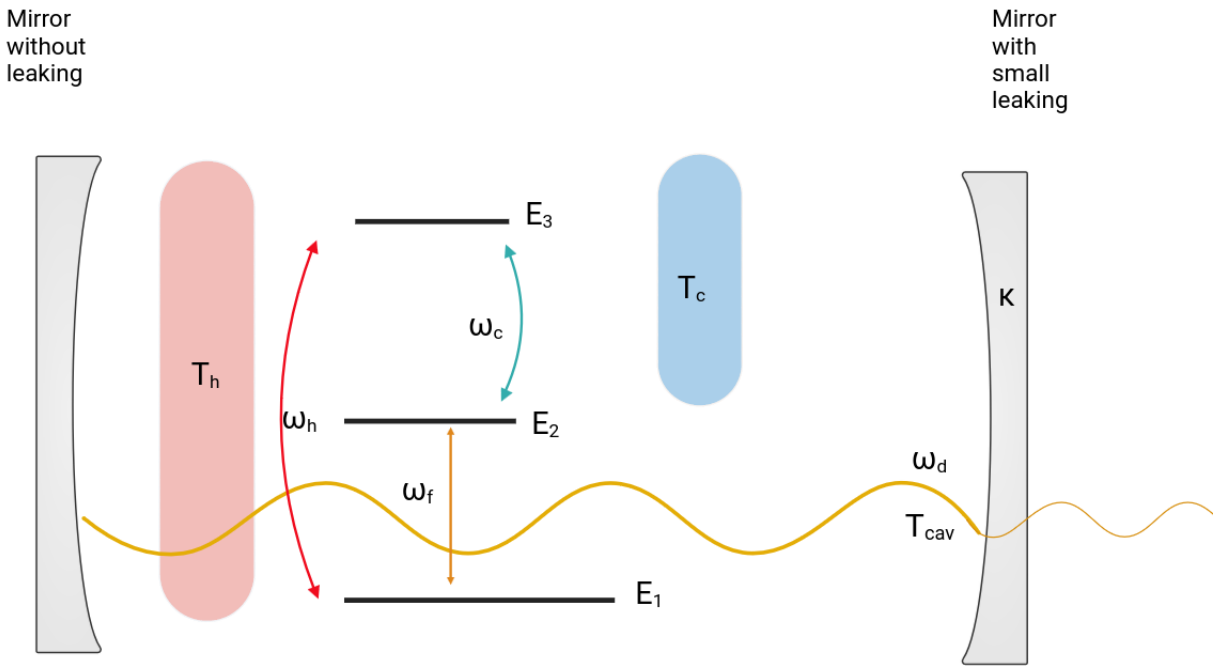

Figure 1: Schematic representation of our three-level laser continuously coupled to two reservoirs of temperatures T_h and T_c. The temperature of the reservoir the cavity couples to is described by T_{cav} The three energy levels are described by the eigenenergies E_1, E_2, E_3. The system is interacting with a quantized single-mode field. The transition frequencies are ω_h, ω_c, ω_f. The leaking from one of the mirrors is given by κ. The frequency of the external field is ω_d. The single mode in the cavity is shown with a yellow line.

A laser produces coherent light, which means all the photons that the laser produces, have the same phase and frequency. The three essential elements of a laser are the gain medium, the pump source, and the cavity, also known as an optical resonator. The gain medium is a material capable of generating and amplifying light. It often consists of material that allows atomic transitions. The gain medium contains at least a three-level system in an excited state and is further excited by the pump mechanism. The pumping mechanism provides the energy to bring the atoms or molecules in the gain medium to the excited state. The energy input causes the atoms or molecules to move to a higher energy state. In our case, it is a thermal bath and an external field. The cavity consists of two mirrors that reflect and amplify the light inside the laser. One of the mirrors is partially transparent to let some of the light out as a laser beam. The resonator reflects the light repeatedly between the mirrors and the light is amplified in the process [5].

Population inversion is a state in which more higher energy levels are occupied than lower energy levels in a system, contrary to their natural distribution. Thus, the pump energy is stored, and a population inversion can be built up. Through stimulated emission by a photon, a second photon will be emitted. This light has the same wavelength and phase as the incident light and further amplifies it. The excited state decays back into the ground state and the cycle can start all over again. To increase the probability that a photon will produce a stimulated photon, that photon must pass through the gain medium several times. Therefore, the laser medium is embedded in a cavity, whereby the photons are reflected. The reflecting in the cavity causes the light to be amplified repeatedly, resulting in an intense, coherent laser beam. These mirrors also finally determine the direction of the generated light beam. One of the two mirrors is designed to be partially transparent so that part of the light can escape and be directed to

its use. Henceforth, in this thesis, we consider a three-level system with three energy levels E_1, E_2, and E_3, embedded in a cavity with frequency ω_{cav}, shown in Fig. 1. We introduce the transition frequencies: $(E_3 - E_1) = \omega_h$, $(E_3 - E_2) = \omega_c$ and the transition $(E_2 - E_1) = \omega_f$ which interacts with the cavity, where $\hbar = 1$. Also, the Boltzmann constant is set to one $k_B = 1$ The Hamiltonian which describes the energy of the three-level system and the cavity mode, without interaction, can be written as follows,

$$H_{free} = \sum_{i=1}^{3} E_i \left|i\right\rangle\!\left\langle i\right| + \omega_{cav} a^\dagger a, \tag{1}$$

where i describes the three different states. The bosonic ladder operators are a and $a^\dagger$ with the commutation relations:$[a, a] = [a^\dagger, a^\dagger] = 0$ and $[a, a^\dagger] = 1$. Our cavity is in resonance with the transition frequency between the states $|1\rangle$ and $|2\rangle$, therefore we set $\omega_{cav} = \omega_f$.

To introduce a phase and drive the cavity we apply a coherent field ω_d, [2]. The strength of the external field is described by f. The Hamiltonian of the external field is

$$V = f(e^{-i\omega_d t} a^\dagger + e^{i\omega_d t} a). \tag{2}$$

A Jaynes-Cummings Hamiltonian models the coupling between the photons and the three-level system,

$$H_{int} = g(\sigma_{12} a^\dagger + \sigma_{21} a), \tag{3}$$

where $\sigma_{12} = |1\rangle\langle 2|$ and $\sigma_{21} = |2\rangle\langle 1|$ are the transition operators. The coupling constant g describes the strength of the coupling between the system and the photons in the cavity. The total Hamiltonian is the sum of (1) (3), (2),

$$H_{tot} = H_{free} + H_{int} + V. \tag{4}$$

The complete description of the system's state at a given time t is encoded in the density matrix $\rho(t)$ [6]. The Lindblad master equation [7] determines its time-evolution

$$\dot{\rho}(t) = \frac{1}{i}[H, \rho] + \mathcal{L}_h \rho + \mathcal{L}_c \rho + \mathcal{L}_{cav} \rho. \tag{5}$$

The first part of Eq.(5) describes unitary time-evolution due to the Hamiltonian. The interaction with the various environmental heat baths is described by the non-unitary part. Open system evolution does not conserve purity. This non-unitary part is described by the Liouvillian

$$\begin{aligned} \mathcal{L}_h \rho &= \frac{\gamma_h}{2}(n_h + 1)\mathcal{D}[\sigma_{13}]\rho + \frac{\gamma_h}{2} n_h \mathcal{D}[\sigma_{31}]\rho, \\ \mathcal{L}_c \rho &= \frac{\gamma_c}{2}(n_c + 1)\mathcal{D}[\sigma_{23}]\rho + \frac{\gamma_c}{2} n_c \mathcal{D}[\sigma_{32}]\rho, \\ \mathcal{L}_{cav} \rho &= \kappa(n_{cav} + 1)\mathcal{D}[a]\rho + \kappa n_{cav} \mathcal{D}[a^\dagger]\rho. \end{aligned} \tag{6}$$

Where $\sigma_{13} = |1\rangle\langle 3|$ is the transition from the ground state to the third state, and $\sigma_{31} = |3\rangle\langle 1|$ describes the transition from the third state to the ground state. The operators σ_{23} and σ_{32} describe the transition from the second to the third state. The coupling of the system and the hot bath is described by $\mathcal{L}_h$, whereas $\mathcal{L}_c$ is the contribution from the coupling with the cold bath coupled with the three-level system. The loss and gain of the photons that are in the cavity, due to finite temperature are described by $\mathcal{L}_{cav}$. Where

$$\mathcal{D}[A]\rho = (2A\rho A^\dagger - A^\dagger A\rho - \rho A^\dagger A). \tag{7}$$

The Bose-Einstein distribution n_h for the hot bath, n_c for the cold bath, and n_{cav} for the distribution of the cavity, determines the average number of photons in the reservoirs

$$n_i = \frac{1}{\exp\left[\frac{\omega_i}{T_i}\right] - 1}. \tag{8}$$

The prefactors $\gamma_c, \gamma_h, \kappa$ describe the spontaneous decay rates.

The working principle of the three-level laser may be understood by considering the following cycle. First, the system is pumped by the hot bath, from the lowest E_1 level to the highest level E_3. From state E_3 the system decays to the lower state E_2 by emitting a photon into the cold bath. From E_2 the decay of the system comes through the stimulated emission of a photon, into the lowest state E_1. This cycle repeats itself and is driven by the thermal gradient between the hot bath with temperature T_h and the cold bath with temperature T_c. As visualized in Fig. 1. The incoming field is also crucial for the heat current. Through stimulated emission, it ensures that photons decay from the averages of the occupation probabilities P_2 to P_1. Thus the external field pushes the cycle on.

3.1 Rotating frame

In thermodynamics, we are often interested in the long-time limit. Therefore the calculations could be done in steady states. The rotating frame is a quantum mechanics technique that transforms a system's Hamiltonian into a rotating reference frame, removing the time-dependent phase factor and simplifying equations. This allows for a more direct analysis of system dynamics in numerical calculations by eliminating time-dependent terms. In our case, the aim is to remove the time-dependent term of the external excitation field of V (2). This method proves particularly useful when the system exhibits rapid oscillations or precession around a specific axis. The derivation of the master-equation in the rotating frame is shown in the appendix (57). The transformation is done with the unitary

$$U = \exp\big(-it(\omega_d a^\dagger a + E_1 |1\rangle\langle 1| + (E_1 + \omega_d) |2\rangle\langle 2| + E_3 |3\rangle\langle 3|)\big). \tag{9}$$

The derivation can be found in the appendix A. The master equation in the rotating frame is

$$\dot{\rho_I}(t) = \frac{1}{i}[H_I, \rho_I] + \mathcal{L}_h\rho_I + \mathcal{L}_c\rho_I + \mathcal{L}_{cav}\rho_I, \tag{10}$$

where $\rho_I = U^\dagger \rho U$ is the density matrix of the system in the rotating frame. The total Hamiltonian in the rotating frame H_I is an ingredient in the master equation in the rotating frame(10). With the detuning $\Delta_1 = \omega_{cav} - \omega_d$ and $\Delta_2 = (E_2 - (E_1 + \omega_d))$, the transformed Hamiltonian can be rewritten as,

$$H_I = H_{int} + f(a^\dagger + a) + \Delta_1 a^\dagger a + \Delta_2 |2\rangle\langle 2|. \tag{11}$$

4 Equations of motion

We study the system dynamics through the Heisenberg equations of motion, which describe the averages of the different time derivatives of the relevant, arbitrary operators $\mathcal{O}$. The equations of motion for the expectation values of the operators in the rotating frame can be calculated as $\partial_t\langle\mathcal{O}\rangle = -i\,\mathrm{Tr}\{[H_I, \mathcal{O}]\rho_I\} + \mathrm{Tr}\{\mathcal{O}\mathcal{L}\rho_I\}$. Solving the equation of motion in the rotating frame allows for the analysis of the dynamics of the three-level laser system, including the average of the occupation probability $\langle p_i\rangle$, the transition operator $\langle\sigma_{ij}\rangle$, and the emission of coherent radiation. The averages of the different time derivatives of the relevant operators are presented in the equations below.

$$\partial_t\langle a\rangle = -i(g\langle\sigma_{12}\rangle + \Delta_1\langle a\rangle + f) - \kappa\langle a\rangle, \tag{12}$$

$$\partial_t\langle p_2\rangle = -ig(\langle\sigma_{21}a\rangle - \langle\sigma_{12}a^\dagger\rangle) + \gamma_c((n_c+1)(1 - \langle p_2 + p_1\rangle) - n_c\langle p_2\rangle), \tag{13}$$

$$\partial_t\langle p_1\rangle = -ig(\langle\sigma_{12}a^\dagger\rangle - \langle\sigma_{21}a\rangle) + \gamma_h((n_h+1)(1 - \langle p_2 + p_1\rangle) - n_h\langle p_1\rangle), \tag{14}$$

$$\begin{aligned}\partial_t\langle\sigma_{12}a^\dagger\rangle = {} & i(g(\langle p_2\rangle + \langle(p_2 - p_1)a^\dagger a\rangle) + f\langle\sigma_{12}\rangle + \Delta_1\langle\sigma_{12}a^\dagger\rangle - \Delta_2\langle\sigma_{12}a^\dagger\rangle) \\ & - \frac{\gamma_h}{2}n_h\langle\sigma_{12}a^\dagger\rangle - \frac{\gamma_c}{2}n_c\langle\sigma_{12}a^\dagger\rangle - \kappa\langle\sigma_{12}a^\dagger\rangle,\end{aligned} \tag{15}$$

$$\partial_t\langle\sigma_{12}\rangle = -ig(\langle(p_1 - p_2)a\rangle) - \frac{\gamma_c}{2}n_c\langle\sigma_{12}\rangle - \frac{\gamma_h}{2}n_h\langle\sigma_{12}\rangle - \Delta_2\sigma_{12}, \tag{16}$$

$$\partial_t\langle a^\dagger a\rangle = -i(g(\langle\sigma_{12}a^\dagger\rangle - \langle\sigma_{21}a\rangle) + f(\langle a^\dagger\rangle - \langle a\rangle)) + 2\kappa(n_{cav} - \langle a^\dagger a\rangle). \tag{17}$$

In Eq. (15) occurs $(p_2 - p_1)a^\dagger a$ and in Eq. (16) occurs $(p_2 - p_1)a$, those factors makes the set of equations not close.

4.1 Factorization

To solve the equations of motion we make an approximation and factorize the $\langle p_1 a^\dagger a\rangle$ and $\langle p_2 a^\dagger a\rangle$ to $\langle p_1\rangle\langle a^\dagger a\rangle$ and $\langle p_2\rangle\langle a^\dagger a\rangle$ and $\langle p_1 a\rangle$ to$\langle p_1\rangle\langle a\rangle$. Nonetheless, errors arise from the applied approximations because the covariance between the ladder operators and the occupation probability is not taken into account. Thus, it can be assumed that the approximations work well in the low-temperature range but not in the high-temperature range where a higher fluctuation occurs. This behavior of deviation is visible in the results of the approximated equations of motion compared to the numerical results, as seen in Fig. 6. Since the approximated term depends on g, one would expect a larger error for a large coupling

constant as well. The separation of the real and the imaginary parts with zero Detuning $\Delta_1 = 0$ and $\Delta_2 = 0$ of those equations gives the equations

$$\partial_t \mathrm{Im}[\langle a\rangle] = -g\mathrm{Re}[\langle\sigma_{12}\rangle] - f - \kappa\mathrm{Im}[\langle a\rangle], \tag{18}$$

$$\partial_t \mathrm{Re}[\langle a\rangle] = g\mathrm{Im}[\langle\sigma_{12}\rangle] - \kappa\mathrm{Re}[\langle a\rangle], \tag{19}$$

$$\partial_t\langle p_2\rangle = -2g(\mathrm{Im}[\langle\sigma_{12}a^\dagger\rangle]) + \gamma_c((n_c+1)(1-\langle p_2+p_1\rangle) - n_c\langle p_2\rangle), \tag{20}$$

$$\partial_t\langle p_1\rangle = 2g(\mathrm{Im}[\langle\sigma_{12}a^\dagger\rangle]) + \gamma_h((n_h+1)(1-\langle p_2+p_1\rangle) - n_h\langle p_1\rangle), \tag{21}$$

$$\begin{aligned}\partial_t\mathrm{Im}[\langle\sigma_{12}a^\dagger\rangle] = {} & g(\langle p_2\rangle + \langle(p_2-p_1)\rangle\langle a^\dagger a\rangle) - f\mathrm{Re}[\langle\sigma_{12}\rangle] \\ & - \frac{\gamma_h}{2}n_h\mathrm{Im}[\langle\sigma_{12}a^\dagger\rangle] - \frac{\gamma_c}{2}n_c\mathrm{Im}[\langle\sigma_{12}a^\dagger\rangle] - \kappa\mathrm{Im}[\langle\sigma_{12}a^\dagger\rangle],\end{aligned} \tag{22}$$

$$\partial_t\mathrm{Re}[\langle\sigma_{12}a^\dagger\rangle] = f\mathrm{Im}[\langle\sigma_{12}\rangle] - \frac{\gamma_h}{2}n_h\mathrm{Re}[\langle\sigma_{12}a^\dagger\rangle] - \frac{\gamma_c}{2}n_c\mathrm{Re}[\langle\sigma_{12}a^\dagger\rangle] - \kappa\mathrm{Re}[\langle\sigma_{12}a^\dagger\rangle], \tag{23}$$

$$\partial_t\mathrm{Im}[\langle\sigma_{12}\rangle] = -g(\langle(p_1-p_2)\rangle\mathrm{Re}[\langle a\rangle]) - \frac{\gamma_c}{2}n_c\mathrm{Im}[\langle\sigma_{12}\rangle] - \frac{\gamma_h}{2}n_h\mathrm{Im}[\langle\sigma_{12}\rangle], \tag{24}$$

$$\partial_t\mathrm{Re}[\langle\sigma_{12}\rangle] = g(\langle(p_1-p_2)\rangle\mathrm{Im}[\langle a\rangle]) - \frac{\gamma_c}{2}n_c\mathrm{Re}[\langle\sigma_{12}\rangle] - \frac{\gamma_h}{2}n_h\mathrm{Re}[\langle\sigma_{12}\rangle], \tag{25}$$

$$\partial_t\langle a^\dagger a\rangle = 2g(\mathrm{Im}[\langle\sigma_{12}a^\dagger\rangle] + 2f\mathrm{Re}[\langle a\rangle] + 2\kappa(n_{cav} - \langle a^\dagger a\rangle). \tag{26}$$

In the case of steady states, where all time derivatives on the left-hand side of the equations are zero, we can resolve them. As described in the appendix (65) and (66), $\mathrm{Im}[\langle\sigma_{12}\rangle]$ give zero, therefore we do not use (18), (22) and (24) for further calculations.

4.2 Approximation for high external field strength f

In the work [2] they analyzed a three-level system without a cavity. We expect for the high f regime a similar behavior of the heat currents as in [2]. To compare the work from [2] with this thesis we are looking for a high f limit, where those two systems are comparable. If the external field f is big compared to the coupling constant g and the impact of g is negligible, we approximate for a steady state , $\langle a\rangle \approx -\frac{-if}{\kappa}$ as described in 18. Out of the equations of motions (20),(21),(24),(25) we derive the approximated equations of motions with set $a = \frac{if}{\kappa}$ for the expectation of the occupation probabilities,

$$\langle p_1\rangle = \frac{\gamma_c\gamma_h\kappa^2 n_c(1+n_h)(\gamma_c n_c+\gamma_h n_h) + 4f^2g^2(\gamma_c+\gamma_h+\gamma_c n_c+\gamma_h n_h)}{\gamma_c\gamma_h\kappa^2(\gamma_c n_c+\gamma_h n_h)(n_c+n_h+3n_c n_h) + 4f^2g^2(\gamma_c(2+3n_c)+\gamma_h(2+3n_h))}, \tag{27}$$

and

$$\langle p_2\rangle = \frac{\gamma_c\gamma_h\kappa^2(1+n_c)n_h(\gamma_c n_c+\gamma_h n_h) + 4f^2g^2(\gamma_c+\gamma_h+\gamma_c n_c+\gamma_h n_h)}{\gamma_c\gamma_h\kappa^2(\gamma_c n_c+\gamma_h n_h)(n_c+n_h+3n_c n_h) + 4f^2g^2(\gamma_c(2+3n_c)+\gamma_h(2+3n_h))}. \tag{28}$$

For the average of $\mathrm{Re}[\langle\sigma_{12}\rangle]$ we get,

$$\mathrm{Re}[\sigma_{12}] = \frac{2fg(n_h-n_c)\gamma_c\gamma_h\kappa}{4f^2g^2((2+3n_c)\gamma_c+(2+3n_h)\gamma_h) + (n_c+n_h+3n_c n_h)\gamma_c\gamma_h(n_c\gamma_c+n_h\gamma_h)\kappa^2}. \tag{29}$$

From the approximated occupation probabilities and the approximated $\langle\sigma_{12}\rangle$, it is possible to express the heat currents as well as the cavity heat current and power. This will be done in section 5.1.1.

4.3 Heat current versus external field

We now have three calculation methods available. Firstly, we can numerically solve the master equation. Secondly, we can numerically solve the average values of the operators out of the equations of motion. Alternatively, we can utilize the purely analytical solutions of the high f approximation. To compare the three different calculation methods with each other we can have a look at Fig. 2 for the current versus the external field. To visualize the power, the calculations are done as in (36) against different values of f and are shown in Fig. 2.

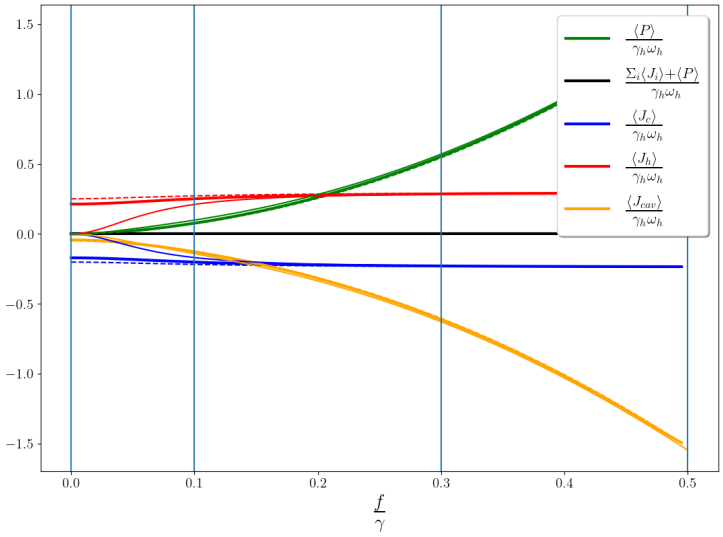

Figure 2: The currents (as calculated with equations (33)-(35)) and the power (as calculated with equation (36)) are shown as a function of the external field strength f. With thick solid lines, the numerical calculations of the master equation are visualized. The high f approximation is shown with thin solid lines. Dashed lines show the numerical solution of the equations of motion. The Bose-Einstein distribution for the hot bath is $n_h = 11$. where the maximum heat current exists. The parameters for the system are expressed with the decay rates γ. The values for all the relevant parameters in the system are $\gamma_c = \gamma_h = \gamma$, $g = 2.8\gamma, \omega_{cav} = 30\gamma, \omega_h = 150\gamma, \omega_c = 120\gamma, n_c = n_{cav} = 0.01, \kappa = 0.2\gamma$. The blue vertical line marks the values of f, for which the Wigner functions are visualized in Fig. 10.

The calculations out of the equations of motion confirm the results from the numerical calculations. If $f > 1.5$, the high f approximation matches the result of the numerics in the high f limit. For small f, a discrepancy is strong. The behavior of the heat current, the cavity heat current, and the power as functions of the external field strength f are examined. Upon observing the heat current $\langle J_h\rangle$ in Fig. 2, it is immediately noticeable that its magnitude remains constant when the Bose-Einstein distribution is around ($n_h \approx 11$). For the cavity heat current and power, a quadratic increase is observed, consistent with the findings in the high-f approximation (40). At high Bose-Einstein distributions, ($n_h > 100$), which occurs after the peak of the double-threshold behavior 6, the influence of f is evident. For the behavior of heat current at very low temperatures, reference is made to the section 7.2, where a cubic increase in heat current is demonstrated.

5 Laws of thermodynamic

5.1 First law of thermodynamic

According to the first law of thermodynamics, the change in internal energy of a closed system is equal to the sum of the change in heat and the change in work. This is illustrated through a graphical representation 3 where the combined values of heat currents and power are plotted. The first law of thermodynamics could be represented by,

$$\Delta U = \Delta Q + \Delta W. \tag{30}$$

It is noteworthy that the sum of the heat currents converges to zero, fulfilling the first law of thermodynamics as shown in Fig. 3. Where U is the internal energy, Q is the heat, and W is the work. To calculate the internal energy, H_{free} is considered [8]. In quantum mechanics, the equation can be rewritten as

$$\partial_t\langle H_{free}\rangle = -i\,\mathrm{Tr}\{[H_{free}, H_I]\rho_I\} + \mathrm{Tr}\{\sum_i (H_{free}\mathcal{L}_i\rho_I)\}. \tag{31}$$

What we get is

$$\partial_t\langle H_{free}\rangle = \langle P\rangle + \langle J_h\rangle + \langle J_c\rangle + \langle J_{cav}\rangle. \tag{32}$$

To calculate the average heat current we evaluate $\mathrm{Tr}\{\mathrm{H}_{\mathrm{free}}\mathcal{L}_{\mathrm{i}}\rho\}$, where the results for the different currents are

$$\langle J_h\rangle = \mathrm{Tr}\{H_{free}\mathcal{L}_h\rho_I\} = \omega_h\gamma_h((n_h)P_1 - (n_h+1)P_3). \tag{33}$$

Similarly, for the cold bath,

$$\langle J_c\rangle = \mathrm{Tr}\{H_{free}\mathcal{L}_c\rho_I\} = \omega_c\gamma_c((n_c)P_2 - (n_c+1)P_3). \tag{34}$$

The result of the cavity heat current is

$$\langle J_{cav}\rangle = \mathrm{Tr}\{H_{free}\mathcal{L}_{cav}\rho_I\} = 2\omega_{cav}\kappa(n_{cav} - \langle a^\dagger a\rangle). \tag{35}$$

J_h is an energy input in the system, therefore it has another sign as J_c and J_{cav}. For the average power, we get

$$\langle P\rangle = -i\mathrm{Tr}\{H_{free}[H_I,\rho_I]\} = -i\omega_{cav}f(\langle a^\dagger\rangle - \langle a\rangle). \tag{36}$$

To get the heat current out of the equations of motion, we express them in terms of the formulas of the occupation probability. The power is given as $\langle P\rangle = -2f\omega_{cav}\mathrm{Im}[\langle a\rangle]$.

5.1.1 Equations of motion

We investigate, whether the equations of motion yield the first law of thermodynamics. The heat currents, the cavity heat current, and the power can be described with the formulas (36) -(33), and are plugged into the equations of motion, yielding:

$$\frac{\langle J_h\rangle}{\omega_h} = -ig(\langle\sigma_{12}a^\dagger\rangle - \langle\sigma_{21}a\rangle) \tag{37}$$

$$\frac{\langle J_c\rangle}{\omega_c} = ig(\langle\sigma_{12}a^\dagger\rangle - \langle\sigma_{21}a\rangle \tag{38}$$

and

$$\frac{\langle J_{cav}\rangle + \langle P\rangle}{\omega_{cav}} = ig(\langle\sigma_{12}a^\dagger\rangle - \langle\sigma_{21}a\rangle). \tag{39}$$

With the condition that $\omega_h = \omega_c + \omega_{cav}$, the sum of the heat currents and the power is zero. therefore, the equations of motion fulfill the first law of thermodynamics.

Out of Eq. (18) the high f approximation $\mathrm{Im}[a] \approx \frac{-g\mathrm{Re}[\sigma_{12}]-f}{\kappa}$, we get the results for the cavity heat current and the power. The approximated result for the cavity heat current with (12) is

$$\frac{\langle J_{cav}\rangle}{\omega_{cav}} \approx 2\Big(n_{cav} - \frac{2fg\mathrm{Re}[\langle\sigma_{12}\rangle] + f^2}{\kappa}\Big), \tag{40}$$

and for the power

$$\frac{\langle P\rangle}{\omega_{cav}} \approx 2\frac{fg\mathrm{Re}[\langle\sigma_{12}\rangle] + f^2}{\kappa}. \tag{41}$$

Note that the approximate formulas (**??**),(**??**),(40),(41) together satisfy the first law of thermodynamic for $n_{cav=0}$, while considering only the first order terms of $\mathrm{Re}[\langle\sigma_{12}\rangle]$. With the formulas (33) and (34) we can express the heat current as follows,

$$\langle J_h\rangle = -\frac{4f^2g^2\gamma_c\gamma_h(-n_c+n_h)\omega_h}{\gamma_c\gamma_h\kappa^2(\gamma_c n_c+\gamma_h n_h)(n_c+n_h+3n_cn_h) + 4f^2g^2(\gamma_c(2+3n_c)+\gamma_h(2+3n_h))}, \tag{42}$$

and

$$\langle J_c\rangle = \frac{\langle J_h\rangle}{\omega_h}\omega_c. \tag{43}$$

In Fig. 3 we verify the adherence to the first law of thermodynamics. The black line represents the sum of heat current, cavity heat current, and power. The sum of the currents and the power is constant zero, which we would expect and validates the first law. The other main statement of Fig. 3 is saturation, where the heat currents $\langle J_h\rangle$ and $\langle J_c\rangle$ initially start from zero. As the coupling strength g increases, the three-level system interacts with photons, preventing the occurrence of cavity heat current and hindering the initiation of the described cycle. However, with an increased g, the cycle can gradually establish the heat currents $\langle J_h\rangle$ and $\langle J_c\rangle$. If the cavity maintains a constant coherent field with a strength f, the cavity heat current and the power exist, also with $g = 0$. The stimulated emission effect from the external field enhances the increase in heat current.

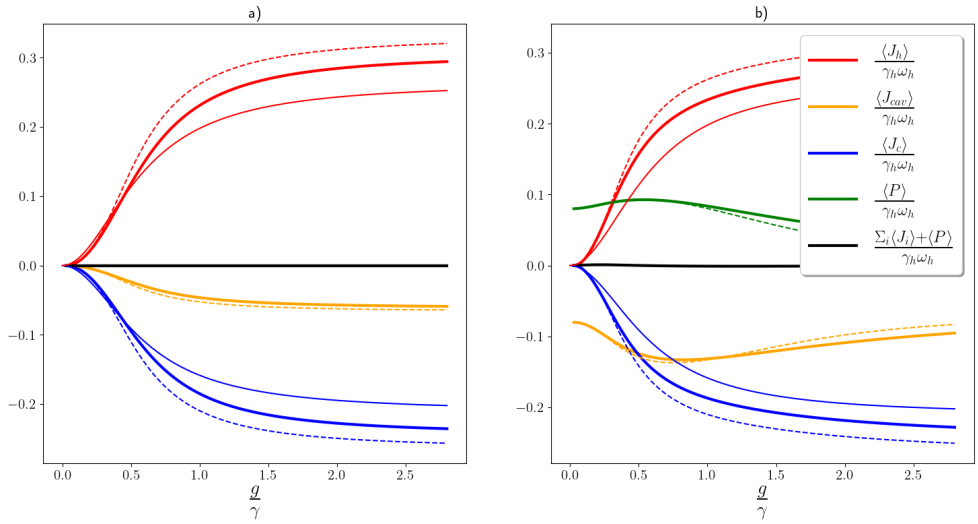

Figure 3: The currents (as calculated with equations (33)-(35)) and the power (as calculated with equation (36)) are shown as a function of the coupling constants g. With thick solid lines, the numerical calculations are visualized. The high f approximation is shown with thin solid lines. Dashed lines show the results of the equations of motion. The Bose-Einstein distribution is set to $n_h = 11$ where the maximum in heat current exist. The parameters for the system are, expressed with the decay rates γ. The values for all the relevant parameters in the system are $\gamma_c = \gamma_h = \gamma$, $g = 2.8\gamma, \omega_{cav} = 30\gamma, \omega_h = 150\gamma$, $\omega_c = 120\gamma, n_h = 11, n_c = n_{cav} = 0.01, \kappa = 0.2\gamma$. The left figure a) shows the results for the $f = 0\gamma$ case. The right figure b) shows the $f = 0.2\gamma$ case.

5.2 Second law

According to the second law of thermodynamics, for an isolated system, the entropy always remains the same or increases but never decreases. In terms of instantaneous quantities, this principle can be expressed through the *entropy production rate* $\dot{\sigma}$, which should always be greater than or equal to zero:

$$\dot{\sigma} \geq 0. \tag{44}$$

Since our focus is on steady-state quantities, we can calculate the entropy production rate by summing up the contributions from heat currents (33)-(35) divided by the respective bath temperature. The formula for the entropy production rate in the steady state is

$$\dot{\sigma} = -\left(\frac{J_c}{T_c} + \frac{J_h}{T_h} + \frac{J_{cav}}{T_{cav}}\right), \tag{45}$$

where S is the von Neumann Entropy. The entropy production rate for different values of n_h is shown in Fig. 4. We observe a distinct maximum at $n_h \approx 11$. The contribution to the entropy production rate from the hot bath is smaller compared to the contribution from the cold bath. This is because the hot bath temperature is much higher, resulting in a smaller value of $\frac{\langle J_h \rangle}{T_h}$ compared to the entropy production rate of the cold bath. By increasing the external field an increased entropy production rate is visible in Fig.4.

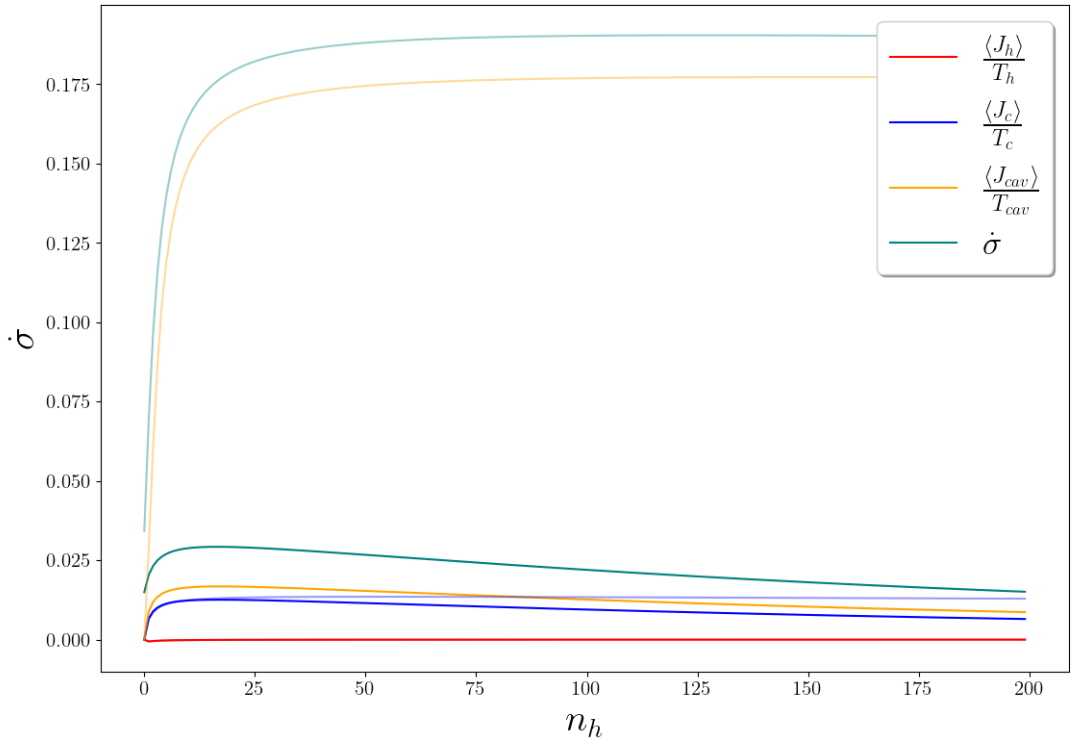

Figure 4: The entropy production rate for different n_h is shown. It is calculated with (45). The non-transparent lines show the $f = 0\gamma$ case. With transparent lines, the numerical results for $f = 0, 2\gamma$ are visualized. The values for all the relevant parameters in the system are $\gamma_c = \gamma_h = \gamma = 1$, $g = 14\kappa$, $\omega_{cav} = 30\gamma$, $\omega_h = 150\gamma, \omega_c = 120\gamma, n_c = n_{cav} = 0.0$, $\kappa = 0.2\gamma$

6 Double-threshold behavior and population inversion

To investigate population inversion, the probability of occupation is calculated as follows, $Tr[|i\rangle \langle i| \rho] = P_i$, where i represents the three different occupation levels. When we increase the Bose-Einstein distribution n_h the population of state $|2\rangle$ is higher than the population of state $|1\rangle$, and a population inversion is observed. It is shown in Fig. 5.

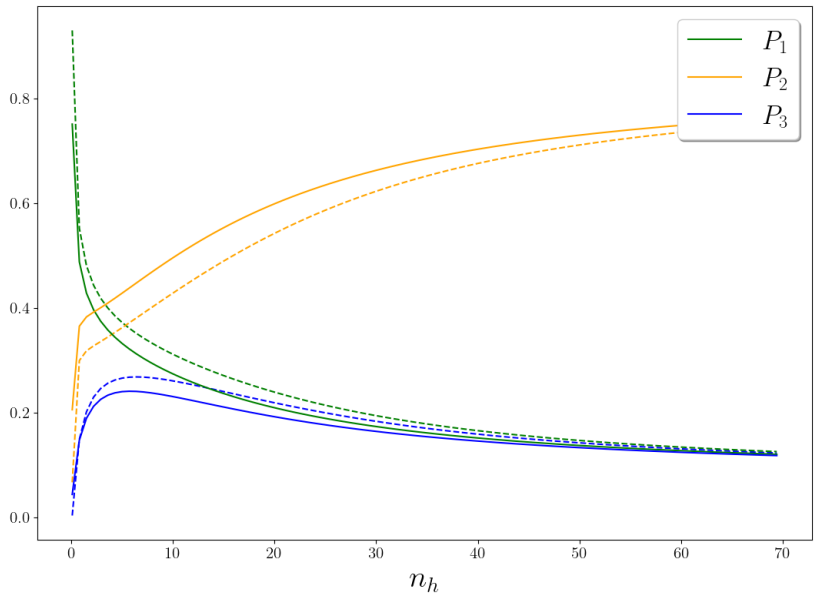

Figure 5: The steady-state probability for the three-level system to stay in a state $|1\rangle, |2\rangle$ or $|3\rangle$ as a function of n_h.The solid lines are the numerical results and the dashed visualize the results out of the equations of motion. The values for all the relevant parameters in the system are $\gamma_c = \gamma_h = \gamma = 1$, $g = 14\kappa, \omega_{cav} = 30\gamma, \omega_h = 150\gamma, \omega_c = 120\gamma, n_c = n_{cav} = 0.02, \kappa = 0.2\gamma$.

In Fig. 6 we observe we are looking at the heat currents. When the hot bath temperature and therefore the Bose-Einstein distribution n_h is relatively low $n_h \approx n_c$, the heat current is low as well and the level E_1 is populated the strongest. By increasing n_h the heat current increases up to a maximum. After reaching the maximum point of heat current we observe a decrease in heat current and entropy production rate. If the heat current is increased excessively, the system will produce thermal light instead of lasing, as shown in Fig. 6.1. This behavior, characterized by an increase followed by a decrease in the heat current as the temperature of the hot bath rises, is referred to as *double-threshold behavior* [6]. To investigate this, we analyze the steady state of the cavity coupled to the three-level system. This behavior can be explained by the *quantum Zeno effect* [9], which suggests that rapid successive measurements can prevent the transition from one state to another. The Zeno effect is experimentally proven and further described in the paper [10] Similarly when sufficient stimulation is applied quickly, the system exhibits similar behavior. The result is, that the heat current stops increasing, and decreases after too much temperature input.

In Fig. 6 the heat current and the power are calculated as a function of the Bose-Einstein distribution n_h. The left figure a) shows the heat current without an external field and the right figure b) shows three different strengths of an external field. With a high external field, $f >> g$ the heat current remains constant as a function for high n_h, visible at the most transparent line in Fig. 6 b). Analytically, the cavity heat current and power are now dependent only on f^2 and are no longer influenced by n_h. We see in Fig. 6 a), a double-threshold behavior in the heat current. The impact of the field for the heat currents J_h and J_{cav} is visible for high Bose-Einstein distributions. But the external field has a bigger influence on the cavity heat current J_{cav}. It is apparent, that the values of the curve with an external field coincide with the curve without an external field until the maximum heat current is reached. After the maximum of the heat current is reached, $n_h \approx 11$, the heat current without the field decreases much faster. Our explanation for the significant increase in heat current is that the external field stimulates more photons from the second energy level $\langle p_2 \rangle$ for emission. This prevents disruption of the cycle at higher temperatures. As a result, the double-threshold behavior is reduced, leading to a higher current of hot current in the high-temperature range. The effect that the external field raises the heat currents could be used to distinguish if the actual temperature is before or after the double-threshold behavior. Further, it can be used to determine which region of temperature we are in. Therefore the difference between the heat current with and without an external field can be used to conclude the temperature. So, we could determine the temperature by measuring the current when the field is switched on or off.

We are in a low-temperature range below the peak if no current difference is detected. After reaching the maximum of the heat current, we see an increasingly larger difference compared to the heat current. This increasing difference could be less prone to errors than measuring the heat current directly and drawing conclusions from it. We thus conclude that a huge external field destroys the double-threshold behavior.

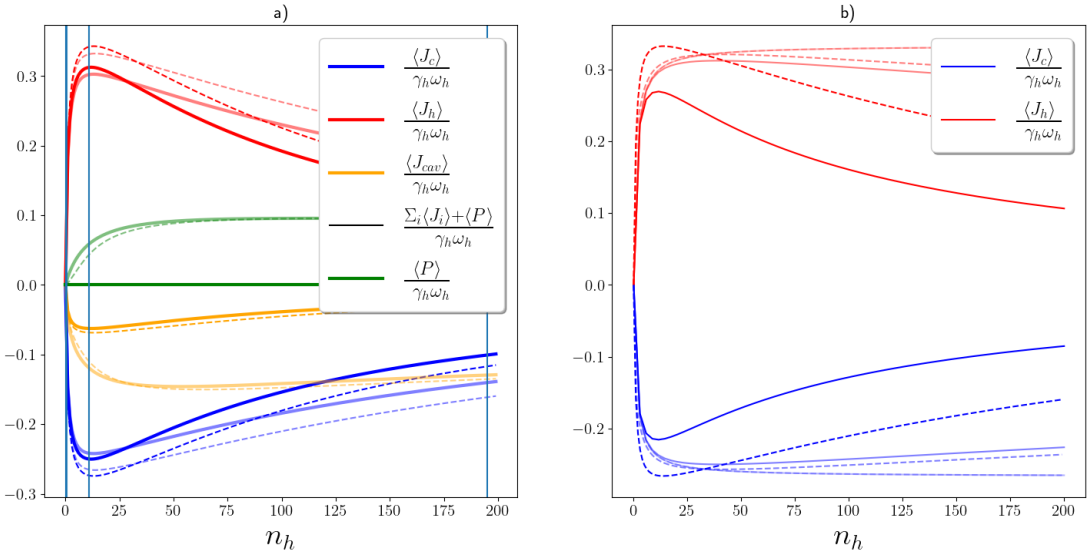

Figure 6: The currents (as calculated with equations (33)-(35)) and the power (as calculated with equation (36)) are shown as a function the Bose-Einstein distributions n_h. With thick solid lines, the numerical calculations are visualized. Dashed lines show the results of the equations of motion. In Fig. a) the heat currents are calculated without an external field (non-transparent lines) and for a small external field strength $f = 0.2\gamma$. In Fig. b) the heat currents (43), (43) for the high f approximation are shown with thin solid lines in the figure. The non-transparent lines show the $f = 0.2\gamma$ case. Semi-transparent lines visualize the calculations for $f = 0.7\gamma$ and the $f = 28\gamma$ case.

Due to the complexity of statements regarding the applications of an external field, the right Fig. 6 b) displays only the solutions of the results for the high f approximation results and the functions of heat current for the high f approximation (42) and (43).

6.1 Wigner functions

In this subsection we analyze the Wigner functions, it is remarkable, that when no external field is applied, the resulting state is similar to a phase average coherent state (PHAV) [11]. We show the Wigner functions for small Bose-Einstein distribution $n_h = 0.1$ where we see something similar to a vacuum state. If we increase the Bose-Einstein distribution, the size of the ring rises as well. We find the largest ring from the PHAV state after the peak of the double-threshold behavior at $n_h = 11$. After reaching the peak, increasing the Bose-Einstein distribution further, the PHAV state disappears and changes to a thermal state. We see these phenomena in the Wigner function Fig. 7 for $n_h = 120$. This is the double-threshold behavior on the Wigner function.

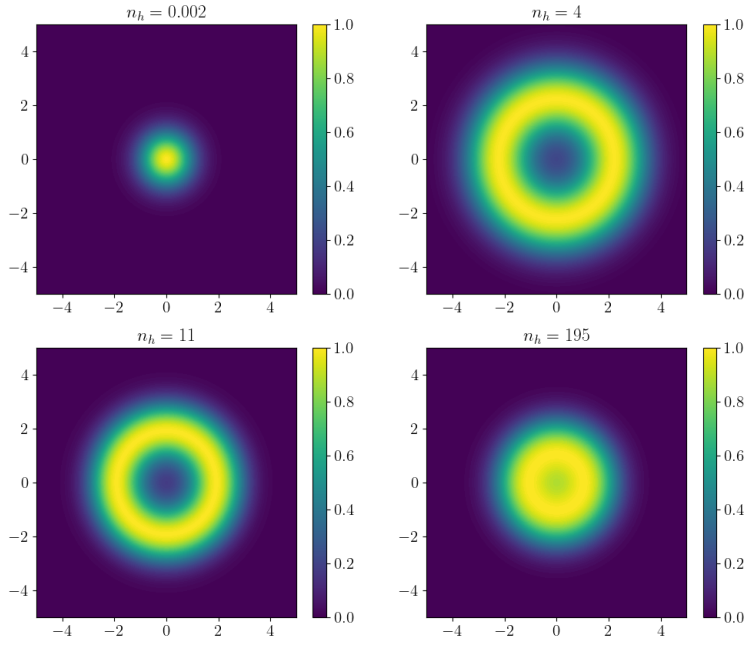

Figure 7: The Wigner functions for four different Bose-Einstein distributions. Those Bose-Einstein distributions are marked with a blue line in Fig. 6. The parameters for the system are, expressed with the decay rates γ. The values for all the relevant parameters in the system are $\gamma_c = \gamma_h = \gamma$, $g = 14\kappa, \omega_{cav} = 30\gamma, \omega_h = 150\gamma, \omega_c = 120\gamma, n_h = 11, n_c = n_{cav} = 0.02, \kappa = 0.2\gamma$.

7 Influence of the external field

7.1 cavity heat current and Power

We are highly interested in the performance of the heat engine and the effective energy/working output of the cavity. The definition of power in quantum heat engines is not yet fully standardized in quantum thermodynamics. Thus, our definition differs from that in [12]. We defined the Energy output with the power without the cavity heat current in the system $\langle J_{cav} \rangle + \langle P \rangle$. By applying an external field, power is induced into the system. Consequently, we are analyzing the difference between the cavity heat current and the power. In Fig. 8 b) without an external field, this corresponds directly to the cavity heat current. With the external field, we observe a difference that peaks at the point of double-threshold behavior.

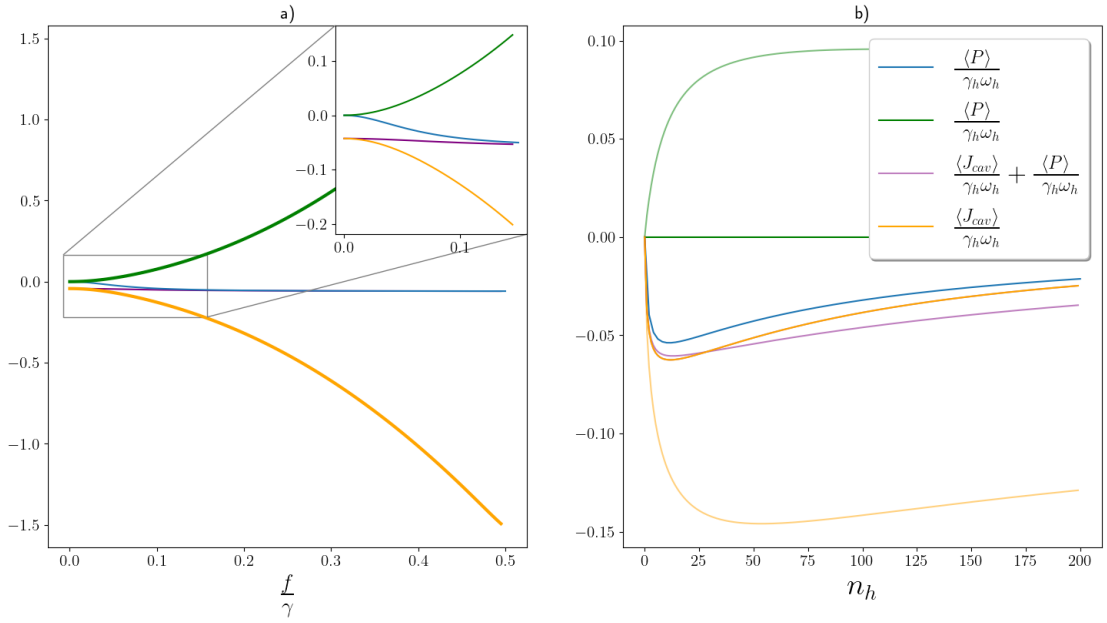

Figure 8: In this figure, the cavity heat current and the power are added together. The parameters for the system are expressed with the decay rate γ. The power, indicated by the light blue line shows the power for the model considered in [2] The values for all the relevant parameters in the system are $\gamma_c = \gamma_h = \gamma, g = 14\kappa, \omega_{cav} = 30\gamma, \omega_h = 150\gamma, \omega_c = 120\gamma, n_h = 11, n_c = n_{cav} = 0.02, \kappa = 0.2\gamma$. In b), the calculations are made for different n_h. In Fig. a) the currents $\langle J_{cav}\rangle$ (35) as well as the power $\langle P\rangle$ (36) for the absence of an external field is visualized and the power plotted as a function of the field strength f. The Bose-Einstein occupation number is set to $n_h = 11$, where the maximum heat current appears.

We observe, that for a strong external field, we get the same output for $\langle J_cav\rangle + \langle P\rangle$ as in [2]. For weak external fields, we get even more power out of the system 8 a).

7.2 Non-linear behavior

From Fig 6, we observed that at $n_h = 0$, a strong external field needs to be applied until we can observe $\langle J_{cav}\rangle$ and $\langle P\rangle$. We found that $\langle J_{cav}\rangle$ and $\langle P\rangle$ are not sensitive to the external field at low temperatures $n_h \approx 0$ but are sensitive at high temperatures. From Eq. (12), we conclude that for the zero temperature $n_h = 0$ our system behaves like a two-level system. Similar to [4], we conclude, that their results are related to our equation of motion. In their work, they obtain the result of the $\langle\sigma_{12}\rangle$ with adiabatic elimination. The result of [4] yield with adiabatically eliminated rewritten in our notation as,

$$\langle\sigma_{12}\rangle = \frac{f}{(2f^2g + g^3)}. \tag{46}$$

If we plug the result for $\langle\sigma_{12}\rangle$ into the equation for $\langle a\rangle$, the following result can be extracted

$$\langle a\rangle = \frac{-i(g\langle\sigma_{12}\rangle + f)}{\kappa} = \frac{-if^3}{g^2 + 2f^2}\kappa. \tag{47}$$

To understand the cubic behavior of the system, we look at the Taylor series. Remarkably, the third-order term is the smallest-order term

$$\langle a\rangle \approx -\frac{2if^3}{g^2\kappa} + \mathcal{O}(f^5). \tag{48}$$

This cubic behavior with the external field f ensures that it needs a strong field to turn on the cavity heat current and that the cavity heat current is unequal to zero by zero temperature. The cubic behavior for the average of the external field $\langle a\rangle$ is seen in Fig. 9 b) where we show with a redline a f^3 curve to compare those two. In [4] they mention that the nonlinearity in a system with a one-dimensional atom primarily arises from two specific characteristics: Firstly, every photon sent into the input field reaches

the two-level system without losses. Secondly, the emitted fluorescence field is directed exclusively into the output ports, preventing leaks and allowing operation at resonance. These features lead to a strong and efficient nonlinear response of the system to incoming photons.

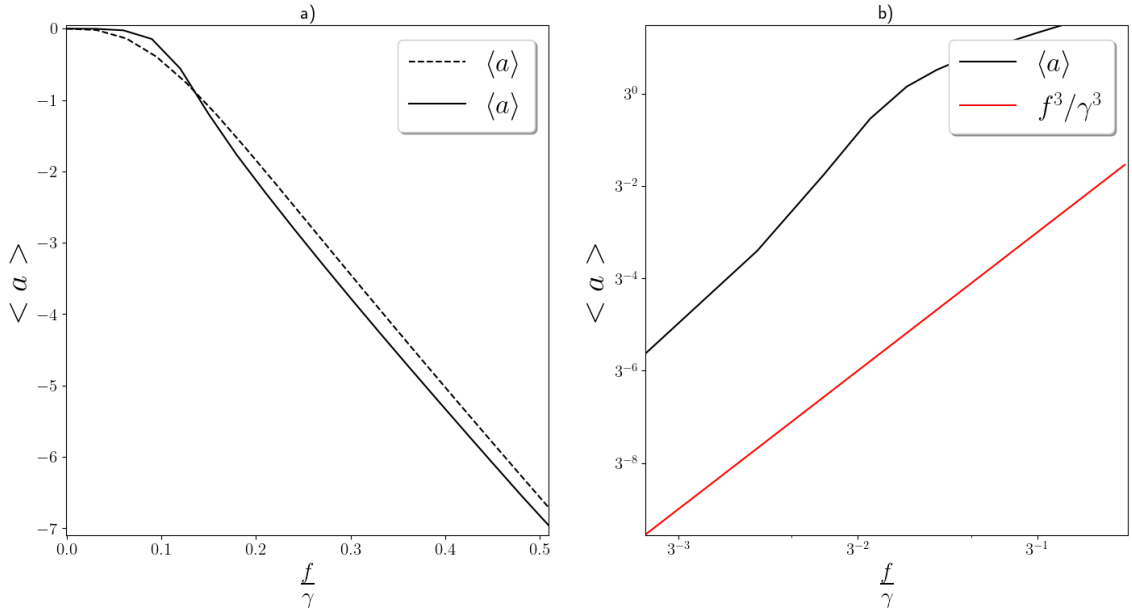

Figure 9: The parameters for the system are, expressed with the decay rates γ. The Frequencies are $\omega_{cav} = 30\gamma, \omega_h = 150\gamma, \omega_c = 120\gamma$ The values for all the relevant parameters in the system are $\gamma_c = \gamma_h = \gamma$, $g = 2.8\gamma, \kappa = 0.2\gamma$ The Bose-Einstein distribution numbers are $n_h = 11, n_c = n_{cav} = 0.02$. In Fig. a), the expected value of a is shown, once numerically with a solid line and once using the analytically derived formula from [4]. On the right side Fig. b), a logarithmic plot is shown, which plots the numerically calculated value logarithmically to the base three. In red, $\frac{f^3}{\gamma^3}$ is calculated to provide a reference line.

This behavior only disappears when the external field is huge compared to g. At a certain sufficiently large value of f, we also have a cavity heat current without any Bose-Einstein distribution difference between the baths. Therefore, there is a cubic behavior value for f that must be exceeded for the expectation value of the lowering operator to be non-zero. This also makes the equation for power (36) non-zero. The explanation for this behavior is described in [4] where they provide exhibits of a giant optical nonlinearity due to the saturation of the two-level system at very low intensities, of the order of one photon per lifetime.

7.3 Wigner function

By injecting a coherent external field, the PHAV state combines with the coherent state, where the probability density relocates from a homogeneous ring to a more and more asymmetric ring, until a banana shape is reached. This banana-shaped state could not be written as a mixed state between a coherent state and a PHAV state. If we increase the external field further, we see a coherent state instead of a PHAV state.

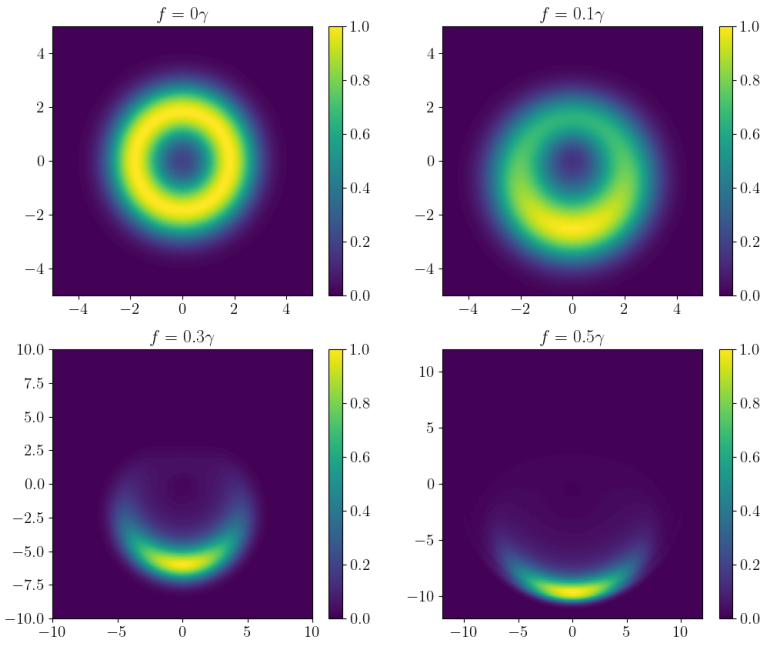

Figure 10: The Wigner functions for four different field strengths f are shown here. The heat currents for those different field strengths are marked with a blue line in Fig. 2. The Bose-Einstein distribution is set to $n_h = 11$ where we have the maximum in entropy production. The parameters for the system are, expressed with the decay rates γ. The Frequencies are $\omega_{cav} = 30\gamma, \omega_h = 150\gamma, \omega_c = 120\gamma$ The values for all the relevant parameters in the system are $\gamma_c = \gamma_h = \gamma$, $g = 14\kappa, \kappa = 0.2\gamma$. The Einstein-Bose occupation numbers are $n_h = 11, n_c = n_{cav} = 0.02$.

8 Thermodynamic Uncertainty Relation

In this section we want to investigate the variance of the current, giving insight into the Thermodynamic Uncertainty Relation (TUR). The thermodynamic uncertainty relation is an important inequality often studied in quantum systems. In our case, we focus on the heat current from the hot bath

$$\frac{\dot{\sigma}}{2} \geqslant \frac{\langle J_h \rangle^2}{\mathrm{Var}(J_h)}. \tag{49}$$

The thermodynamic uncertainty relation itself is derived from the large deviation rate function and the generalized thermodynamic forces. From this force, the entropy production rate can be classically calculated. Near equilibrium, the typical fluctuations are known to be Gaussian with a variance that is twice the mean value[13]. Violations of the TUR have been observed in various quantum systems, such as several quantum heat engines [2] and [14]. The TUR provides insights into the fundamental limits of precision in thermodynamic measurements in the quantum regime. It highlights the trade-off between the accuracy of heat and entropy measurements and the impact of quantum fluctuations on these measurements.

8.1 Full counting statistics

To investigate the TUR, we need to determine the variance of the heat current. For this purpose, the Fullcounting statistic is suitable. This is a mathematical framework that allows us to examine the statistical properties of events or transmitted quantities. The counting field χ serves as an auxiliary variable in the master equation to facilitate the calculation of moment-generating functions (e.g., mean, variance, or higher cumulants) of counting events. By differentiating the generating function, which depends on the Counting Field, concerning this field and then setting the field to zero, the desired statistical sizes can be derived. We introduce the density matrix with this counting field as follows:

$$\rho(\chi) = \sum_{n}^{\infty} e^{it\chi} \rho(n), \tag{50}$$

with $\rho(n)$ the resolved density matrix. Overall, full counting statistics provides a powerful tool for understanding and quantifying the statistical behavior of counting processes in various physical systems, ranging from quantum transport to stochastic processes in classical systems. Its applications have proven to be crucial in fields such as quantum mechanics. The formalism of full counting statistics can be derived in different ways. Here, the calculations are based on moment-generating functions and their derivatives, similar to the generating field in quantum field theory encodes the statistical properties of the counting process. By manipulating these generating functions, one can extract valuable information about the system, such as the average current, and the variance. The moment-generating function is

$$M(\chi, t) = \mathrm{Tr}\{e^{\mathcal{L}_\chi t} \rho\}, \tag{51}$$

with the tilted Liouvillian, which satisfies the following equation

$$\partial_t \rho_\chi = \mathcal{L}_\chi \rho_\chi(t). \tag{52}$$

To check the thermodynamic uncertainty relation, we choose the variance of the current J_h, which could be calculated in general with the two-point correlation function, or in our cases with moment-generating functions. The n-th moment of a random variable is defined as the expected value of the n-th power of the random variable. As shown in [3] we need a moment generating function for the current J_h to investigate the variance of our system. In our specific case, if we analyze the heat current, the tilted Liouvillian is

$$\mathcal{L}(\chi) = e^{-i\chi\omega_h} \frac{\gamma_h}{2}(n_h + 1)(\sigma_{31}\rho\sigma_{31}^\dagger - \{\sigma_{31}^\dagger\sigma_{31}, \rho\}) + e^{i\chi\omega_h} \frac{\gamma_h}{2}(n_h)(\sigma_{31}\rho\sigma_{31}^\dagger - \{\sigma_{31}^\dagger\sigma_{31}, \rho\}) + \mathcal{L}_c + \mathcal{L}_{cav}. \tag{53}$$

The partial derivative concerning χ from $\mathcal{L}(\chi)$ corresponds to the current, and therefore we introduce the first-moment generating function

$$i\partial_\chi \mathcal{L}(\chi)\rho|_{\chi=0} = \omega_h \frac{\gamma_h}{2}(n_h + 1)(\sigma_{13}\rho\sigma_{13}^\dagger) + \omega_h \frac{\gamma_h}{2}(n_h)(\sigma_{31}\rho\sigma_{31}^\dagger). \tag{54}$$

It is also possible to express the heat current as $\mathrm{Tr}\{H_{free}\mathcal{L}_h\rho\} = \mathrm{Tr}\{J\rho\}$. But for the variance, we also need the second derivative of the moment-generating function.

$$\partial_\chi^2 \mathcal{L}(\chi)\rho|_{\chi=0} = \omega_h^2 \frac{\gamma_h}{2}(n_h+1)\sigma_{13}\rho\sigma_{13}^\dagger + \omega_h^2 \frac{\gamma_h}{2}(n_h)\sigma_{31}\rho\sigma_{31}^\dagger. \tag{55}$$

For more information about the calculation with the tilted Liouvillian please refer to [3]. Finally the variance $Var(J_h)$ is then given as

$$Var(J_h) = -\mathrm{Tr}\{\partial_\chi^2\mathcal{L}\rho\} - 2\,\mathrm{Tr}\{\partial_\chi\mathcal{L}\partial_\chi\rho_\chi\} + 2\,\mathrm{Tr}\{\partial_\chi\mathcal{L}\rho_\chi\}\,\mathrm{Tr}\{\partial_\chi\rho_\chi\}. \tag{56}$$

To implement the variance in a numerically efficient way, vectorization is used in the implementation of the equation (56). Further details can be found in the appendix C.1

8.2 TUR investigations

To visualize the TUR Eq. 49 is rewritten as $\mathcal{Q} = \dot{\sigma}\frac{Var\langle J_h\rangle}{\langle J_h\rangle^2}$. Where $\mathcal{Q} \geq 2$ for the classical limit. To examine for which parameter the TUR is violated, it is necessary to look at the coupling constant g, the strength of the field f, and the Bose-Einstein distributions n_h, n_c, and n_f.

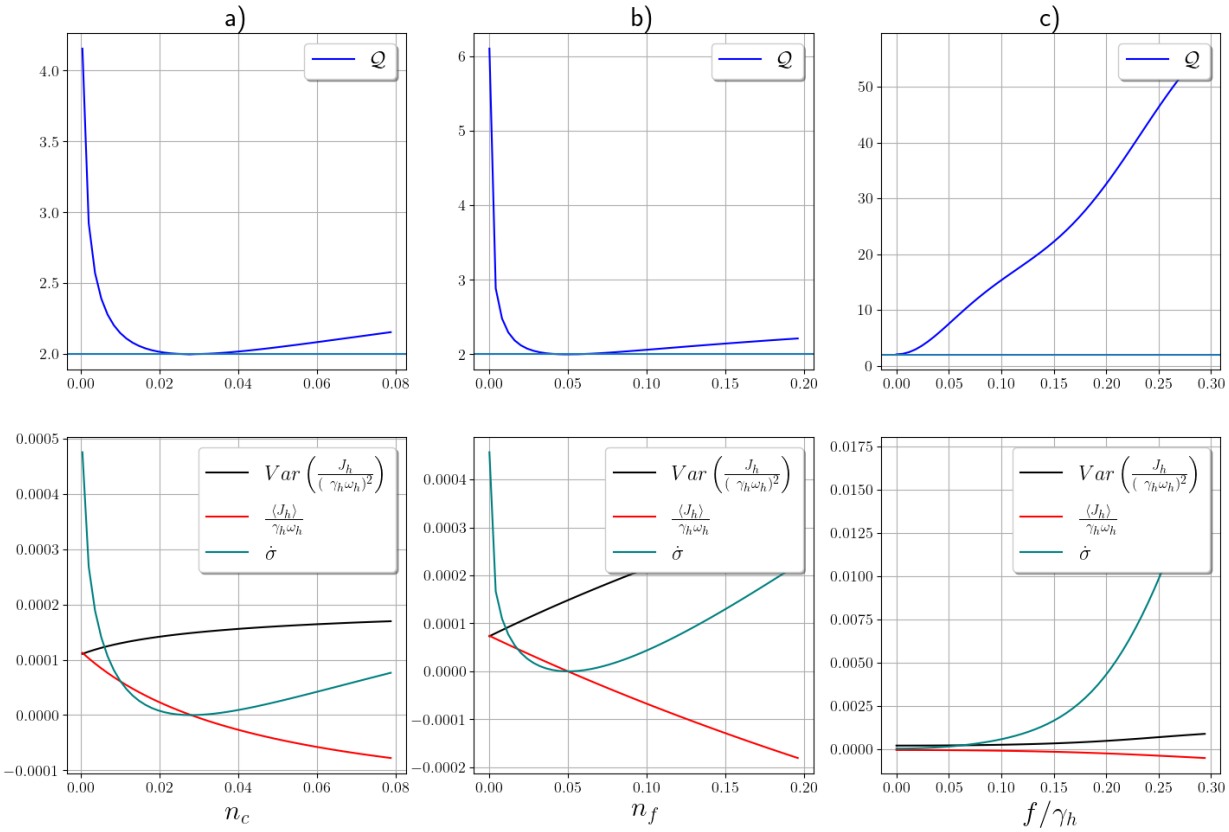

Figure 11: On the three upper figures, the $\mathcal{Q}$ factor is shown as a function of three different parameters. The TUR limit of 2 is marked with a horizontal blue line. Below each image, the entropy production rate, the average heat current $\langle J_h\rangle$, and the variance $Var(J_h)$ are separately presented. The energies of the levels of the system are expressed with $E_1 = 0\gamma_h, E_2 = 30\gamma_h, E_3 = 150\gamma_h$. The Bose-Einstein distributions are $n_h = 0.013, n_c = 0.027, n_f = 0.07$, and the decay rates from the atomic transition are expressed in terms of γ_h. The decay rate from the cold bath transition is set to $\gamma_c = 20\gamma_h$. The decay rate from the cavity is $\kappa = 0.002\gamma_h$, and the coupling constant is $g = 2.8\gamma_h$. The external field is set to zero $f = 0\gamma_h$.

When looking at Fig. 11 a), where the factor $\mathcal{Q}$ is visualized against n_c, it is noticeable that the minimum of $\mathcal{Q}$ occurs only at the reversal regime of the heat current. The reversal regime of the heat current is the regime where the heat current changes direction. Therefore the heat current changes its sign, as opposed to reference [2], where the TUR is violated away from the reverse regime. At the reversal point of the heat current, there is also the lowest entropy production rate, which, increases significantly with an increase in the Bose-Einstein factor, leading to $\mathcal{Q}$ being always greater than two. The same phenomenon occurs when considering Fig. 11 b). Here, again, the factor $\mathcal{Q}$ approaches the TUR limit of 2 closely, without surpassing it. In both cases, machine inaccuracies occur at the minima of $\mathcal{Q}$, making it difficult to gather precise information. In Fig. 11 c), the factor $\mathcal{Q}$ is shown as a function of the external field f. It's noticeable, that the entropy increases significantly, indicating a corresponding increase in $\mathcal{Q}$. The variance and the heat current increase slowly. The main message from this figure is that as the external field increases, $\mathcal{Q}$ increases as well. In [2], a three-level system is driven solely by an external field $H = \epsilon(e^{i\omega t}\sigma_{12} + e^{-i\omega t}\sigma_{21})$, which is plotted in Fig. 12. For our system, we can translate in the

high f approximation to $\epsilon = \frac{fg}{\kappa}$. The TUR and the currents of this system were calculated analytically. Additionally, an analytical equation for the variance and the TUR was found. In [2], there is no cavity present. To better compare their system and results with ours, we will calculate the values for the high f limit and large cavity leaking, which brings it closer to the behavior without a cavity. To make the values comparable, the different Hamiltonians were compared, and κ and g were set so that at the high f limit, $f = 20\gamma_h$ is achieved. The factor $\mathcal{Q}''$ describes the TUR factor from [2]. To match the minimum of the $\mathcal{Q}''$ factor, we set $\frac{fg}{\kappa} = 0.15$, aligning with the value of ϵ at which the peak TUR violation is observed, as reported in [2]. To better investigate how the TUR behaves without the entropy production rate of the cavity and whether it aligns with $\mathcal{Q}''$, we plotted our TUR factor $\mathcal{Q}$ without $\frac{\langle J_{cav}\rangle}{T_{cav}}$, therefore $\dot{\sigma} = \frac{\langle Jh\rangle}{T_h} + \frac{\langle J_c\rangle}{T_c}$ as $\mathcal{Q}'$.

In [2], a stronger TUR violation was found with asymmetric decay rates $\gamma_c = 20\gamma_h$. With asymmetric decay rates ($\gamma_h \neq \gamma_c$), we observe TUR violations without considering the entropy production of the cavity, as shown in Fig. 12a)

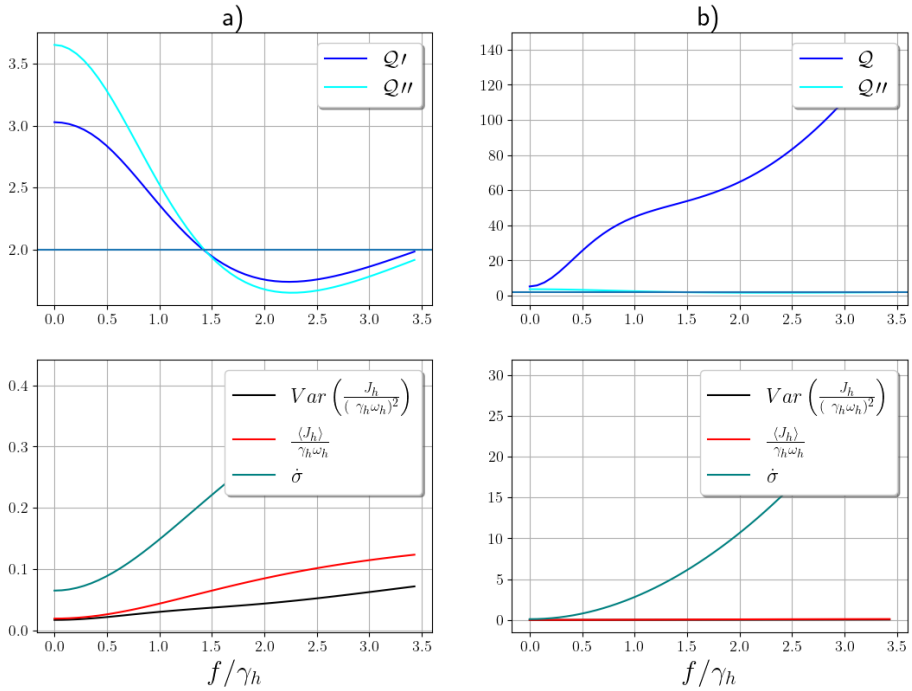

Figure 12: In the upper figures, the $\mathcal{Q}'$ factor is shown as a function of f. The TUR limit of 2 is marked with a horizontal blue line. Below each image, the entropy production rate, the heat current J_h, and the variance $Var(J_h)$ are separately presented. The energies of the levels of the system are $\omega_1 = 0\gamma_h, \omega_2 = 30\gamma_h, \omega_3 = 150\gamma_h$. The Bose-Einstein distributions are $n_h = 5, n_c = 0.027, n_f = 0.07$, The decay rate cold bath from the atomic transition is $\gamma_c = 20\gamma_h$. The decay rate from the cavity is $\kappa = 0.2$, and the coupling constant is $g = 0.15$. The $\mathcal{Q}''$ factor, which is drawn with the light blue line, shows the reference curve from [2] In a) the calculations for $\mathcal{Q}'$ are done without the entropy production rate of the cavity. Therefore $\dot{\sigma} = \frac{\langle J_h\rangle}{T_h} + \frac{\langle J_c\rangle}{T_c}$. In Fig. b) the calculations are done with the full entropy production rate given in 45.

In Fig. a), The curve behaves similarly when the entropy coming from the cavity is not included shown by the curve $\mathcal{Q}'$. In Fig. b), the $\mathcal{Q}$ factor is calculated with the total entropy production rate, and what is immediately noticeable is, that the cavity produces too much entropy to violate the TUR. The aquamarine line represents $\mathcal{Q}$ as calculated in the paper [2]. We observe that under these conditions, fewer TUR violations occur, but the curve behaves similarly. The parameters, which also exist in [2], are the same; however, the Hamiltonian in our system differs from that presented in this paper. We came closer to the TUR limit $\mathcal{Q} \approx 2$ with small values of κ. Interestingly, the TUR is violated strongest before the peak of the double-threshold behavior. After reaching the peak of double-threshold behavior, the

state approaches a thermal state. We can assume through our observation, that a thermal state doesn't violate the TUR. The impact of the entropy production rate for an external field unequal zero is also visible in Eq. 4.

To better visualize the effect of detuning, it is necessary to activate the external field. To make conclusions effectively for a small detuning, we opted for a field of $f = 0.1\gamma_h$. Under these conditions, there is no longer any violation of the TUR. However, it is evident that even a slight detuning leads to an increased TUR factor $\mathcal{Q}$.

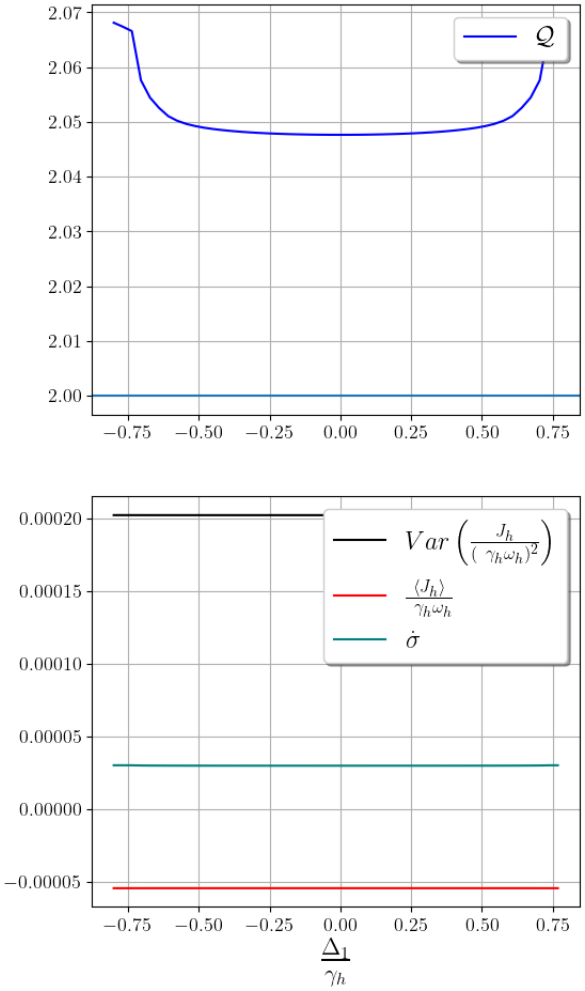

Figure 13: This figure shows $\mathcal{Q}$ as a function of the detuning between the cavity and the external field (Δ_1). The energies of the levels of the system are $E_1 = 0\gamma_h, E_2 = 30\gamma_h, E_3 = 150\gamma_h$. The Bose-Einstein distributions are $n_h = 5, n_c = 0.027,\ n_f = 0.07$, the decay rates from the atomic transitions are $\gamma_h = 0.1$ and $\gamma_c = 2$. The decay rate from the cavity is $\kappa = 0.002\gamma_h$, and the coupling constant is $g = 2.8\gamma_h$. The external field is set to $f = 0.1\gamma_h$.

In summary, we can say that under variation of all parameters, no violation of TUR was found. The variance and the entropy production rate of the heat current increase significantly with increasing temperature in a three-level system in a cavity. Minima in the TUR is found only in the reverse regime, and even then, these minima do not fall below the classical TUR limit. By turning on a coherent external field in combination with the cavity, the entropy production rate increases much more than the heat current itself. Especially the ratio $\frac{\langle J_{cav}\rangle}{T_{cav}}$ increases so much that the TUR cannot be violated anymore.

9 Conclusion

In this thesis, we were able to make predictions about how the heat current and the cavity current behave in our quantum heat engine. For this purpose, we started to find three different methods of a three-level system driven by a thermal bath and an external field. First, we calculated the heat currents numerically and then found a set of the Heisenberg equations of motion and solved them numerically. The third way was to approximate the equations of motion for the high f regime to solve them analytically. All methods matched each other. To investigate the behavior of the heat current in the system, it represents the heat current as a function of the strength of the external field, the coupling constant, and the Bose-Einstein distribution. We could compare our results for the high f regime with [2] and for the case of $n_h = 0$ as a two-level system and his behavior with [4] and could verify the non-linear behavior of the cavity heat current.

In the second part of this work, the focus was on the TUR. Full counting statistics was used to calculate the variance, which was done in two different ways. From the variance, we calculated the TUR factor $\mathcal{Q}$. We analyzed the result of $\mathcal{Q}$ for all the relevant parameters in the Master equation.

We identified various quantum properties of the heat current as a function of the Bose-Einstein distribution n_h, the external field f, and the coupling constant g. While observing the heat current as a function of the Bose-Einstein distribution, a double-threshold behavior as reported in [6], is visible. Increasing the external field or coupling constant also led to an increase in the heat current. When increasing g we observed saturation of the heat current. Increasing the external field f resulted in a quadratic increase, without any saturation behavior. We found that at low temperatures, turning the external field on and off doesn't change the heat current. However, at high temperatures, the effect of the external field is significant. If the temperature is higher than the peak temperature of the double-threshold behavior, the heat current remains constant under temperature variation. Thus, conclusions about the temperature can be seen from observing the heat current 6. It is important to mention that the heat current behaves very similarly to power, and statements about power can be made by considering the heat current. Comparing the power with findings reported in [2], it can be seen that the model in this work generates more power output for a small external field. This is due to the cavity influencing the cavity heat current. For a strong external field, we reach the same limit. This comparison illustrates how different external conditions and models can lead to varied thermodynamic and power behaviors, with the properties of the external field and its interaction with the system being crucial variables. We also demonstrated that this three-level laser does not violate the classical TUR limit with adjusted parameters. In comparison to the work performed in [2], we do not observe a violation of the TUR here. Although there are clear minima in the TUR factor $\mathcal{Q}$, compared to the temperatures, in our case, the minimum of $\mathcal{Q}$ occurs in the reverse regime and precisely at $\mathcal{Q} = 2$. We assume that the external field produces too much entropy, as was visible in figure 11 c), where the entropy increases quadratically.

Further evaluation of the difference between the heat current with and without an external field could indicate, whether we are below or above the double-threshold. Furthermore, applications in thermometry could be possible. Theoretical investigations have already been conducted on the violation of TUR with entangled qubits. However [14], it has not been conclusively determined whether the TUR is more or less violated when the qubits are entangled or not. Entanglement is a quantum mechanical phenomenon where two or more particles are so interconnected that the state of one particle immediately depends on that of the other, regardless of the spatial separation between them. Hence, it would be intriguing for us to conduct more precise investigations in the future on multiple entangled three-level systems within a cavity to explore TUR violation. As a first step, implementing the entangled system as described in [14] but into a cavity and examining TUR violation would be crucial. Such proposals have already been suggested for implementations using three-level atoms, which could then be experimentally realized. [15] Further possibilities to violate the TUR might involve introducing a single-mode squeezed state instead of an external coherent field.

Commentary on the use of AI

The text of this thesis was written by myself. To improve my text, I used Grammarly (AI-based so far as I understood that), which I integrated into my browser on the advice of Marcelo Janovitch. It provided spelling and grammar suggestions, as well as occasional sentence restructuring. For the translation of more complex sentences, I used DeepL and other AI-based translators in a few passages. The order of referencing corresponds to the frequency with which I have used them.
https://www.deepl.com/translator
https://app.grammarly.com/
https://chat.openai.com/

References

[1] H. E. Scovil and E. O. Schulz-Dubois, "Three-level masers as heat engines," *Physical Review Letters*, vol. 2, no. 6, pp. 262–263, Mar. 1959. [Online]. Available: `https://link.aps.org/doi/10.1103/PhysRevLett.2.262`.

[2] A. A. S. Kalaee, A. Wacker, and P. P. Potts, "Violating the thermodynamic uncertainty relation in the three-level maser," *Physical Review E*, vol. 104, no. 1, pp. 1–12, 2021.

[3] G. T. Landi, M. J. Kewming, M. T. Mitchison, and P. P. Potts, "Current fluctuations in open quantum systems: Bridging the gap between quantum continuous measurements and full counting statistics," pp. 1–59, 2023. [Online]. Available: `http://arxiv.org/abs/2303.04270`.

[4] A. Auffèves-Garnier, C. Simon, J. M. Gérard, and J. P. Poizat, "Giant optical nonlinearity induced by a single two-level system interacting with a cavity in the Purcell regime," *Physical Review A - Atomic, Molecular, and Optical Physics*, vol. 75, no. 5, pp. 1–16, 2007.

[5] M. Sargent, M. O. Scully, and W. E. Lamb, *Laser physics*. 2018, pp. 1–432.

[6] S. W. Li, M. B. Kim, G. S. Agarwal, and M. O. Scully, "Quantum statistics of a single-atom Scovil-Schulz-DuBois heat engine," *Physical Review A*, vol. 96, no. 6, pp. 1–10, Oct. 2017. [Online]. Available: `http://arxiv.org/abs/1710.00902%20http://dx.doi.org/10.1103/PhysRevA.96.063806`.

[7] G. Lindblad, "On the generators of quantum dynamical semigroups," *Communications in Mathematical Physics*, vol. 48, no. 2, pp. 119–130, 1976.

[8] T. Sagawa, "Quantum Thermodynamics," *SpringerBriefs in Mathematical Physics*, vol. 16, pp. 89–115, 2022.

[9] B. Misra, *The Zeno's paradox in quantum theory*, 1977. [Online]. Available: `http://repository.ias.ac.in/51139/`.

[10] W. M. Itano, D. J. Heinzen, J. J. Bollinger, and D. J. Wineland, "Quantum Zeno effect," *Physical Review A*, vol. 41, no. 5, pp. 2295–2300, 1990.

[11] A. Allevi, M. Bondani, P. Marian, T. A. Marian, and S. Olivares, "Characterization of phase-averaged coherent states," *Journal of the Optical Society of America B*, vol. 30, no. 10, p. 2621, 2013.

[12] J. Monsel, M. Fellous-Asiani, B. Huard, and A. Auffèves, "The Energetic Cost of Work Extraction," *Physical Review Letters*, vol. 124, no. 13, pp. 1–6, 2020.

[13] T. R. Gingrich, J. M. Horowitz, N. Perunov, and J. L. England, "Dissipation Bounds All Steady-State Current Fluctuations," *Physical Review Letters*, vol. 116, no. 12, pp. 1–5, 2016.

[14] K. Prech *et al.*, "Entanglement and thermokinetic uncertainty relations in coherent mesoscopic transport," *Physical Review Research*, vol. 5, no. 2, pp. 1–22, 2023.

[15] A. del Rio-Lima, F. J. Poveda-Cuevas, and O. Castaños, "Entanglement of a three-level atom interacting with two-modes field in a cavity," pp. 1–37, 2024. [Online]. Available: `http://arxiv.org/abs/2401.04892`.

[16] X. Zhang and X. Sheng, "Two methods for computing the Drazin inverse through elementary row operations," *Filomat*, vol. 30, no. 14, pp. 3759–3770, 2016.

A Rotating frame transformation

In this section of the appendix, our focus lies on the transformation of the master equation into the rotating frame. To derive the master equation with the density matrix in the rotating frame, we begin by multiplying out the chain rule from the left side of the equation. As a result, we observe the emergence of two new terms in the equation. Remark, $\gamma_5, \gamma_6 = \kappa$ in this derivation

$$\begin{aligned}
&i\partial t\rho_I = (\partial_t U^\dagger)\rho U + U^\dagger(\partial_t\rho)U + U^\dagger\rho(\partial_t U)\\
&= (\partial_t U^\dagger)\rho U + U^\dagger(-i[H,\rho] + \sum_i \gamma_i(2A_i\rho A_i^\dagger - A_i^\dagger A_i\rho - \rho A_i^\dagger A_i))U + U^\dagger\rho(\partial_t U)\\
&= \partial_t U^\dagger\rho U + U^\dagger\rho\partial_t U - i(U^\dagger HUU^\dagger\rho U - U^\dagger\rho UU^\dagger HU)\\
&+ \sum_i^6 \gamma_i(n_i+1)/2(2U^\dagger A_i UU^\dagger\rho UU^\dagger A_i^\dagger U - U^\dagger A_i^\dagger UU^\dagger A_i UU^\dagger\rho U\\
&- U^\dagger\rho UU^\dagger A_i^\dagger UU^\dagger A_i U))\partial_t U^\dagger UU^\dagger\rho U + U^\dagger\rho UU^\dagger\partial_t U - i[U^\dagger HU,\rho_I]\\
&+ \sum_i^6 \gamma_i(n_i+1)/2(2(U^\dagger A_i U)\rho_I(U^\dagger A_i^\dagger U) - (U^\dagger A_i^\dagger U)(U^\dagger A_i U)\rho_I)\\
&+ \sum_i^6 \gamma_i n_i/2(2U^\dagger A_i UU^\dagger\rho UU^\dagger A_i^\dagger U - U^\dagger A_i^\dagger UU^\dagger A_i UU^\dagger\rho U\\
&- U^\dagger\rho UU^\dagger A_i^\dagger UU^\dagger A_i U))\partial_t U^\dagger UU^\dagger\rho U + U^\dagger\rho UU^\dagger\partial_t U - i[U^\dagger HU,\rho_I]\\
&+ \sum_i^6 \gamma_i n_i/2(2(U^\dagger A_i U)\rho_I(U^\dagger A_i^\dagger U) - (U^\dagger A_i^\dagger U)(U^\dagger A_i U)\rho_I)
\end{aligned} \tag{57}$$

Above the transformation of the unitary part of the master equation is shown. In the first line the chain role from the partial derivation of the density matrix is applied.
Then the chain rule acts on the right part of the master equation.
In the third line, the commutator is expanded.
To simplify the equation, the property $\mathbb{1} = U^\dagger U$ is used.

$$\begin{aligned}
&i\partial t\rho_I = -i(U^\dagger HU + i\partial tU^\dagger U)\rho_I + i\rho_I(U^\dagger HU + i\partial tU^\dagger U)\\
&+ \sum_i \gamma_i(n_i+1)\mathcal{D}[U^\dagger A_i U]\rho_I + \sum_i \gamma_i n_i/2\mathcal{D}[U^\dagger A_i U]\rho_I\\
&= -i[(U^\dagger HU + i(\partial_t U^\dagger)U,\rho_I] + \sum_i \gamma_i(n_i+1)U^\dagger\mathcal{D}[A_i]U\rho_I + + \sum_i \gamma_i(n_i+1)/2U^\dagger\mathcal{D}[A_i]U\rho_I + \sum_i \gamma_i n_i/2U^\dagger\mathcal{D}[A_i]U\rho_I.
\end{aligned} \tag{58}$$

Therefore the new Hamiltonian for the rotating frame has to be:$H_I = U^\dagger HU + i(\partial tU^\dagger)U$

The transformation of the operators to the rotating frame is listed below, the calculations come from the Baker-Campbell-Hausdorff-formula.

$$\begin{aligned}
U^\dagger\sigma_{12}U &= e^{-i\omega_d t}\sigma_{12},\\
U^\dagger\sigma_{21}U &= e^{i\omega_d t}\sigma_{21},\\
U^\dagger aU &= e^{-i\omega_d t}a,\\
U^\dagger a^\dagger U &= e^{i\omega_d t}a^\dagger.
\end{aligned} \tag{59}$$

After the transformation, the different parts of the Hamiltonian are given as

$$U^\dagger VU = f(a + a^\dagger), \tag{60}$$

$$U^\dagger H_{free}(\partial_t U^\dagger)U = \Delta_1 a^\dagger a + \Delta_2 |2\rangle\langle 2|, \tag{61}$$

$$U^\dagger H_{int}U = g(\sigma_{12}a^\dagger + \sigma_{21}a). \tag{62}$$

It is also necessary to transform the non-unitary part of the von Lindblad equation.

$$U\mathcal{D}[A]U^\dagger = \mathcal{D}[UAU^\dagger]\rho_I = (2UAU^\dagger\rho_I UA^\dagger U^\dagger - UA^\dagger U^\dagger UAU^\dagger\rho_I - \rho_I UA^\dagger U^\dagger UAU^\dagger). \tag{63}$$

When we insert the operators A from the transformation (59) we get:

$$\mathcal{D}[UAU^\dagger]\rho_I = (2e^{-i\omega_d t}A\rho_I e^{+i\omega_d t}A^\dagger) - (e^{i\omega_d t}A^\dagger e^{-i\omega_d t}UAU^\dagger\rho_I) - (\rho_I e^{i\omega_d t}A^\dagger e^{-i\omega_d t}A). \tag{64}$$

Here, A is one of the operators from Eq. (59), where A is an arbitrary system operator. Because the dissipative part (59) includes term with $AA^\dagger$, the time-dependent terms of $e^{-i\omega_d t}$ and $e^{i\omega_d t}$ cancel each other. Therefore, the unitary transformation to the rotating frame has no effect, yielding $U^\dagger \mathcal{D}[A]\rho U = \mathcal{D}[A]\rho$.

B Equations of motion

In case of steady states without a external field ($f = 0\gamma$) and if the parameters Δ_1, Δ_2 are set to zero, Eq. (18) yields

$$\mathrm{Re}[\langle\sigma_{12}\rangle] = -\frac{\mathrm{Im}[\langle a\rangle]\kappa}{g}, \tag{65}$$

out of Eq. (19)

$$\mathrm{Im}[\langle\sigma_{12}\rangle] = \frac{\mathrm{Re}[\langle a\rangle]\kappa}{g}. \tag{66}$$

From Eq. (22), we can make a conclusion about $\mathrm{Re}[\langle a\rangle]$ with following calculations:

$$\mathrm{Im}[\langle\sigma_{12}\rangle] = -\frac{2\mathrm{Re}[\langle a\rangle]g\langle p_1 - p_2\rangle}{n_c\gamma_c + n_h\gamma_h} \tag{67}$$

$$\frac{\mathrm{Re}[\langle a\rangle]\kappa}{g} = -\frac{2\mathrm{Re}[\langle a\rangle]g\langle p1 - p2\rangle}{n_c\gamma_c + n_h\gamma_h} \Rightarrow \mathrm{Re}[\langle a\rangle] = 0 \tag{68}$$

From Eq. (66) we see that also $\mathrm{Im}[\langle\sigma_{12}\rangle]$ has to be zero. With equation (23) follows, that

$$\mathrm{Re}\langle\sigma_{12}a^\dagger\rangle = \frac{2f\mathrm{Im}\langle\sigma_{12}\rangle}{n_c\gamma_c + n_h\gamma_h + 2\kappa} \Rightarrow \mathrm{Re}\langle\sigma_{12}a^\dagger\rangle = 0 \tag{69}$$

The analytical result for $\langle a^\dagger a\rangle$ with the parameters $\gamma_h = \gamma_c = \gamma$ is given as

$$\begin{aligned}
\langle a^\dagger a\rangle = {} & \frac{1}{(8g^2(2+n_c+2n_h)(4+3n_c+3n_h)\gamma^2\kappa)}(-((2+n_c+2n_h)\gamma^2((n_c+n_h+3n_cn_h)\gamma\kappa \\
& (n_c\gamma+n_h\gamma+2\kappa)+2g^2(4\kappa-8n_{cav}\kappa+n_c(\gamma+2\kappa]-6n_{cav}\kappa)-n_h \\
& (\gamma-4\kappa+6n_{cav}\kappa)))) \\
& +((2+n_c+2n_h)^2\gamma^4((n_c+n_h+3n_cn_h)^2\gamma^2\kappa^2(n_c\gamma+n_h\gamma+2\kappa)^2 \\
& +4g^4((n_c-n_h)^2\gamma^2+4(nc^2(1-3n_{cav}+6n_h)+n_c(2-4n_{cav}+15n_h+6n_h^2) \\
& +n_h(6+4n_h+n_{cav}(4+3n_h)))\gamma\kappa+4(2+n_c+4n_{cav}+3n_cn_{cav}+2n_h+3n_{cav}n_h)^2\kappa^2) \\
& +4g^2(n_c+n_h+3n_cn_h)\gamma\kappa(n_c\gamma+n_h\gamma+2\kappa)(-n_h\gamma+4\kappa+8n_{cav} \\
& \kappa+4n_h\kappa+6n_{cav}n_h\kappa+n_c(\gamma+2\kappa+6n_{cav}\kappa))))^{\frac{1}{2}}).
\end{aligned} \tag{70}$$

The analytical solution for the occupation probabilities $\langle p_1\rangle$ and $\langle p_2\rangle$ if $\gamma = 1$ and $n_{cav}, n_c = 0$ are

$$\begin{aligned}
\langle p_1\rangle = {} & -\Big(\frac{1}{8g^2n_h(4+3n_h)}\Big)(2+n_h)(\kappa n_h(2\kappa+n_h)+g^2(-4n_h+8\kappa(1+n_h)) \\
& +\sqrt{\kappa^2n_h^2(2\kappa+n_h)^2+8g^2\kappa n_h(2\kappa+n_h)(-n_h+2\kappa(1+n_h))}+ \\
& \sqrt{16g^4(n_h^2+4\kappa^2(1+n_h)^2+4\kappa n_h(3+2n_h))}),
\end{aligned} \tag{71}$$

and

$$\begin{aligned}
\langle p_2\rangle = {} & \Big(\frac{1}{4g^2n_h(4+3n_h)}\Big)(4g^2(2\kappa(1+n_h)^2+n_h(3+2n_h))+ \\
& (1+n_h)(\kappa n_h(2\kappa+n_h)+\sqrt{\kappa^2n_h^2(2\kappa+n_h)^2+8g^2\kappa n_h(2\kappa+n_h)(-n_h+2\kappa(1+n_h))}+ \\
& \sqrt{16g^4(n_h^2+4\kappa^2(1+n_h)^2+4\kappa n_h(3+2n_h))})).
\end{aligned} \tag{72}$$

C Full counting statistics

C.1 Vectorisation

To make full counting statistics numerically, we need to perform our calculations in a vectorized form. This enables the usage of the algebraic relation shown in Eq. (79)

$$vec\left(\begin{bmatrix} a & b \\ c & d \end{bmatrix}\right) = \begin{bmatrix} a \\ c \\ b \\ d \end{bmatrix}. \tag{73}$$

With this vectorization, we could rewrite the Liouvillian with its eigenvectors and eigenvectors

$$\mathcal{L} = \sum_{j\neq 0} \lambda_j |x_j\rangle\!\rangle\langle\!\langle y_j|. \tag{74}$$

The matrix exponential can be rewritten as

$$e^{\mathcal{L}t} = |\rho\rangle\!\rangle\langle\!\langle \mathbb{1}| + \sum_{j\neq 0} e^{\lambda_j t} |x_j\rangle\!\rangle\langle\!\langle y_j|. \tag{75}$$

We introduce the pseudo inverse, the Drazin inverse, defined as

$$\mathcal{L}^+ = \int_0^\infty d\tau e^{\mathcal{L}\tau}(1 - |\rho\rangle\!\rangle\langle\!\langle \mathbb{1}|) = \sum_{j\neq 0} \frac{1}{\lambda_j} |x_j\rangle\!\rangle\langle\!\langle y_j|, \tag{76}$$

where we invert the non-zero eigenvalues. For a more detailed description, please refer to [3]

With the Drazin inverse, we can rewrite equation (56) as follows. For short notation, we call the first derivative the superoperator of the moment generating function Eq.(54) $\mathcal{J}$ and the second derivative Eq. (55) K

$$Var(J) = K - 2\langle\!\langle \mathbb{1}|\mathcal{J}\mathcal{L}^+\mathcal{J}|\rho\rangle\!\rangle. \tag{77}$$

A fast way to implement the Drazin inverse is described in the paper [16].

This approach is applicable for computing higher cumulants, whereas, for the specific task of computing variances in higher-dimensional Hilbert spaces, we have opted for a more efficient technique. In pursuit of faster implementation, we have found it advantageous to bypass the direct computation of the Drazin inverse. Instead, it is faster to calculate the product of $\mathcal{L}^+\mathcal{J}|\rho\rangle\!\rangle = |z\rangle\!\rangle$ in the vectorized form directly with the following (d^2+1) dimensional equation

$$\begin{pmatrix} \vdots \\ \mathcal{L} \\ \vdots \\ \langle\!\langle \mathbb{1}| \end{pmatrix} |z\rangle\!\rangle = \begin{pmatrix} \vdots \\ \mathcal{J}|\rho\rangle\!\rangle - |\rho\rangle\!\rangle\langle\!\langle \mathbb{1}|\mathcal{J}|\rho\rangle\!\rangle \\ \vdots \\ 0 \end{pmatrix}. \tag{78}$$

With algebraic property

$$\mathrm{Vec}(ABC) = (C^T \otimes A)|B\rangle\!\rangle, \tag{79}$$

This calculation yields $\mathcal{J}\,|z\rangle\rangle = \sum_i^3 \nu_k (\sigma_{ij})^T \otimes \sigma_{ij}\,|z\rangle\rangle$, where $|z\rangle\!\rangle = \mathcal{L}^+\,|\alpha\rangle\rangle$. Solving this equation for $|z\rangle\!\rangle$, we can use the next equation to get the variance $Var(J)$ of the current.

The two superoperators $\mathcal{L}$ and $\mathcal{J}$ mapped to matrices, while ρ behaves like a vector. Eq. (**??**) leads to a significant simplification of all formulas, as a result speeding up their numerical computation.

The variance from the current is then given by

$$Var(J) = K - 2\langle\!\langle \mathbb{1}|\mathcal{J}|z\rangle\!\rangle \tag{80}$$

We calculate the variance by implementing the Drazin inverse of the Liouvillion and compare the resulting variance with the variance calculated by the second, faster, method, where the Drazin inverse is not calculated explicitly.

University of Basel

Faculty of Science

Declaration on Scientific Integrity
(including a Declaration on Plagiarism and Fraud)
Translation from German original

Title of Thesis: The thermodynamic uncertainty relation in the three-level laser with a quantized field

Name Assessor: Dr. Patrick Potts

Name Student: Sander Stammbach

Matriculation No.: 17-052-523

I attest with my signature that I have written this work independently and without outside help. I also attest that the information concerning the sources used in this work is true and complete in every respect. All sources that have been quoted or paraphrased have been marked accordingly.

Additionally, I affirm that any text passages written with the help of AI-supported technology are marked as such, including a reference to the AI-supported program used. This paper may be checked for plagiarism and use of AI-supported technology using the appropriate software. I understand that unethical conduct may lead to a grade of 1 or "fail" or expulsion from the study program.

Place, Date: Sissach, 30.4.2024 Student:

Will this work, or parts of it, be published?

☐ No

☑ Yes. With my signature I confirm that I agree to a publication of the work (print/digital) in the library, on the research database of the University of Basel and/or on the document server of the department. Likewise, I agree to the bibliographic reference in the catalog SLSP (Swiss Library Service Platform). (cross out as applicable)

Publication as of: April 30 2024

Place, Date: Sissach, 30.4.2024 Student:

Place, Date: Basel, 29.04.2024 Assessor: 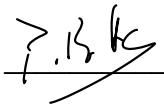

Please enclose a completed and signed copy of this declaration in your Bachelor's or Master's thesis.